JEM Journal of Experimental Medicine

ARTICLE

# ACC1-expressing pathogenic T helper 2 cell populations facilitate lung and skin inflammation in mice

Takahiro Nakajima[1], Toshio Kanno[1], Satoru Yokoyama[1], Shigemi Sasamoto[1], Hikari K. Asou[1], Damon J. Tumes[2], Osamu Ohara[3], Toshinori Nakayama[4,5], and Yusuke Endo[1,6]

**T cells possess distinguishing effector functions and drive inflammatory disorders. We have previously identified IL-5–producing Th2 cells as the pathogenic population predominantly involved in the pathology of allergic inflammation. However, the cell-intrinsic signaling pathways that control the pathogenic Th2 cell function are still unclear. We herein report the high expression of acetyl-CoA carboxylase 1 (ACC1) in the pathogenic CD4⁺ T cell population in the lung and skin. The genetic deletion of CD4⁺ T cell–intrinsic ACC1 dampened eosinophilic and basophilic inflammation in the lung and skin by constraining IL-5 or IL-3 production. Mechanistically, ACC1-dependent fatty acid biosynthesis induces the pathogenic cytokine production of CD4⁺ T cells via metabolic reprogramming and the availability of acetyl-CoA for epigenetic regulation. We thus identified a distinct phenotype of the pathogenic T cell population in the lung and skin, and ACC1 was shown to be an essential regulator controlling the pathogenic function of these populations to promote type 2 inflammation.**

## Introduction

Allergic diseases including atopic dermatitis (AD) and asthma have been increasing worldwide and are a significant public problem in most developed countries. These disorders are driven by type 2 cytokines, including IL-4, IL-5, and IL-13 derived from T helper 2 (Th2) cells and type 2 innate lymphoid cells (ILC2s; Fahy, 2015; Guttman-Yassky et al., 2011; Nakayama et al., 2017). Recently, tissue-derived checkpoint cytokines including IL-25, IL-33, and thymic stromal lymphopoietin secreted from injured epithelial cells and keratinocytes have also been implicated in Th2-associated diseases through their amplification of Th2 cytokine-mediated responses (Holgate, 2012) and driving IL-5 and IL-13 production by ILC2s.

We previously identified IL-33–dependent IL-5–producing allergen-specific pathogenic Th2 (Tpath2) cells in allergic eosinophilic airway inflammation (Endo et al., 2014; Nakayama et al., 2017). IL-5 is critical for generation, recruitment to inflammatory sites, and activation of eosinophils (Dougan et al., 2019) that play a key role for severe asthma and chronic AD (Aleman et al., 2016; Islam et al., 2011). IL-13 induces IgE production by B cells, tissue fibrosis, and mucus production in the airways (Brandt and Sivaprasad, 2011; Gour and Wills-Karp, 2015), decreases expression of skin structural proteins, and induces itchiness in AD. T cell–derived IL-3 is also involved in skin inflammation via basophil activation and migration (Leyva-Castillo et al., 2013).

Mammalian target of rapamycin (mTOR) integrates the signaling pathways associated with nutrient levels, energy status, cell stress, and growth factor–mediated signaling (Saxton and Sabatini, 2017). Emerging evidence has demonstrated that metabolic reprogramming toward an anabolic phenotype during naive-to-effector T cell differentiation is coordinated by mTOR signaling. The absence of mTORC1 signaling inhibits naive CD4⁺ T cell differentiation into effector cells (Delgoffe et al., 2009). mTOR complex 2 (mTORC2) induces Th2 cell differentiation by inhibiting suppressor of cytokine signaling 5 (SOCS5), which represses IL-4–dependent STAT6 signaling (Stark et al., 2019). In contrast, the suppression of both mTORC1 and mTORC2 promotes differentiation of induced regulatory T cells (Chapman and Chi, 2014). Thus, mTOR plays a pivotal role in orchestrating metabolic programs during T cell differentiation, with

[1]Department of Frontier Research and Development, Laboratory of Medical Omics Research, Kazusa DNA Research Institute, Chiba, Japan; [2]Centre for Cancer Biology, University of South Australia, North Terrace, Adelaide, Australia; [3]Department of Applied Genomics Kazusa DNA Research Institute, Chiba, Japan; [4]Department of Immunology, Graduate School of Medicine, Chiba University, Chiba, Japan; [5]AMED-CREST, AMED, Chiba, Japan; [6]Department of Omics Medicine, Graduate School of Medicine, Chiba University, Chiba, Japan.

Correspondence to Yusuke Endo: endo@kazusa.or.jp.

mTORC1 and mTORC2 exerting distinct effects on downstream molecular signaling. The abrogation of mTOR signaling with rapamycin also reportedly suppresses the function of ILC2s in vitro and alleviates IL-33–induced airway inflammation in vivo (Salmond et al., 2012).

Altered lipid metabolism is required for the early activation of CD4$^+$ T cells via mTOR-mediated alterations to fatty acid synthesis (Angela et al., 2016). De novo fatty acid synthesis is initiated by the activation of sterol regulatory element-binding protein 1 (SREBP-1; Stark et al., 2019), which mediates the proliferation and controls the function of CD8$^+$ T cells through the transcriptional regulation of acetyl-CoA (Ac-CoA) carboxylase α (ACC1, the gene product of *Acaca*; Lee et al., 2014). ACC1, a rate-limiting enzyme of fatty acid biosynthesis, contributes to Th17 cell differentiation in mouse and human obesity (Endo et al., 2015a), directs cell fate decisions during memory CD4$^+$ T cell generation, and positively regulates follicular helper cell numbers in vivo (Endo et al., 2019). The fatty acid uptake program is also crucial for activation of T cells and maintenance of tissue-resident memory T cells (Angela et al., 2016; Pan et al., 2017). However, while mounting evidence has highlighted the importance of lipid metabolism for T cell differentiation and function, the role of T cell lipid metabolism in allergic diseases remains unclear.

We herein show that ACC1 drives two distinct pathogenic T cell populations to facilitate allergic inflammation in vivo. We found that the numbers of ST2$^+$ IL-5–producing Tpath2 cells in the lung and eosinophilic airway inflammation were dependent on ACC1. Similarly, genetic deletion of ACC1 abrogated MC903-induced skin inflammation by inhibiting the production of IL-3 by skin CD4$^+$ T cells. Mechanistically, ACC1-mediated de novo fatty acid biosynthesis controlled the maximal activation of glycolysis, which is required for IL-5 production by Tpath2 cells. Our study therefore indicates that ACC1 is an essential metabolic regulator that controls the inflammatory function of pathogenic CD4$^+$ T cells in the lung and skin.

## Results

### IL-5–producing Tpath2 cells express high levels of ACC1

In previous studies, we discovered a population of IL-5$^{high}$-expressing memory Th2 cells in an OVA antigen–specific model of memory Th2 cell formation. These cells were ST2$^{hi}$CXCR3$^{lo}$CD62L$^{lo}$, and we named them pathogenic memory Th2 (Tpath2) cells (Endo et al., 2015b; Endo et al., 2014; Endo et al., 2011) owing to their heightened ability to induce eosinophilic airway inflammation. We further found that IL-33 signaling via ST2 in memory Th2 cells greatly enhances the Tpath2 phenotype (high IL-5 production) and confers pathogenicity to antigen-specific memory Th2 cells in eosinophilic airway inflammation in both mice and humans (Endo et al., 2015b). We therefore use the term Tpath2 to refer to memory CD4$^+$ T cells that produce the cytokine IL-5, have cell surface expression of ST2, respond to IL-33, and are pathogenic in terms of the induction of eosinophilic airway inflammation. Although IL-33–ST2 signaling is known to contribute to phosphoinositide 3-kinase–mediated mTOR activation, resulting in the regulation of metabolic homeostasis (Weichhart et al., 2015), its role in the pathogenicity of Th2 cells and allergic inflammation remains poorly understood.

To investigate the role of mTOR signaling in the induction of Tpath2 cells, we first analyzed memory Th2 cells prepared as demonstrated in Fig. S1 A (Endo et al., 2011). We use the name "antigen-specific Tpath2 cells" for in vivo–generated OVA antigen–specific ST2$^{hi}$ memory Th2 cells exposed to IL-33. We use the term "polyclonal Tpath2 cells" for cells that were not antigen specific but resembled memory (CD44$^{hi}$CD62L$^{lo}$) CD4$^+$ T cells and consisted of the polyclonal population of cells with the Tpath2 phenotype. The phosphorylation of 4EBP1 and S6 ribosomal protein, which are major downstream molecules of mTOR signaling, was significantly up-regulated in response to IL-33 stimulation (Fig. 1 A). As reported previously, we confirmed that IL-33 induced the production of IL-5 and IL-13 by antigen-specific Tpath2 cells and polyclonal Tpath2 cells (Fig. S1 B; Endo et al., 2015b; Yamamoto et al., 2018). Rapamycin, a pharmacologic inhibitor of mTOR signaling, clearly suppressed the IL-33–mediated augmentation of IL-5 and IL-13 in antigen-specific Tpath2 and polyclonal Tpath2 cells (Fig. 1, B and C). In contrast, IL-4 production was slightly decreased by rapamycin (Fig. S1, C and D). Similarly, the mRNA expression of *Il5* and *Il13* was significantly decreased by rapamycin treatment (Fig. 1, D and E). These results suggested that IL-33–mediated mTOR activation was crucial for the induction of IL-5–producing Tpath2 cells.

We previously reported that ACC1-mediated fatty acid biosynthesis is required for the early activation and proliferation of naive and memory CD4$^+$ T cells (Angela et al., 2016). Furthermore, we and other groups have reported using CD4-Cre$^+$*Acaca*$^{fl/fl}$ (hereafter *Acaca*$^{-/-}$) mice that Th17 cells are highly dependent on the de novo fatty acid biosynthesis pathway (Berod et al., 2014; Endo et al., 2015a). These previous findings suggest that the fatty acid biosynthesis pathway may also be involved in the differentiation of Tpath2 cells. Thus, we next analyzed the expression of ACC1 in lung lymphocytes from healthy mice. We found that ST2$^{hi}$ IL-5–producing cells were predominantly detected in the ACC1$^{hi}$ population and rarely observed in the ACC1$^{int}$ or ACC1$^{lo}$ populations (Fig. S1 E). IL-33 treatment strongly increased IL-5–producing ACC1$^{hi}$ lymphocytes in the lung (Fig. S1 F). Furthermore, in IL-33–treated inflammatory lungs, most of the ST2$^{hi}$ IL-5–producing cell population consisted of TCRβ$^+$CD4$^+$ polyclonal Tpath2 cells and ILC2s (TCRβ$^-$CD4$^-$), whose ACC1 protein expression was higher than ST2$^{lo}$IL-5$^-$ and ST2$^{hi}$IL-5$^-$ cell populations (Fig. 1, F and G). We also found that IL-33 treatment resulted in the up-regulation of genes related to the fatty acid biosynthesis pathway, including *Acaca*, *Elovl1*, *Elovl5*, *Fads2*, *Scd1*, *Scd2*, *Acsl3*, and *Fasn* in Tpath2 cells (Fig. 1 H and Fig. S1 G). The inhibition of mTOR by rapamycin treatment suppressed the up-regulation of fatty acid biosynthesis genes in antigen-specific Tpath2 and polyclonal Tpath2 cells (Fig. 1 I and Fig. S1 G). Taken together, these results suggest that IL-33–mediated mTOR activation induces fatty acid biosynthesis, which enables Th2 cells to differentiate into IL-5–producing Tpath2 cells.

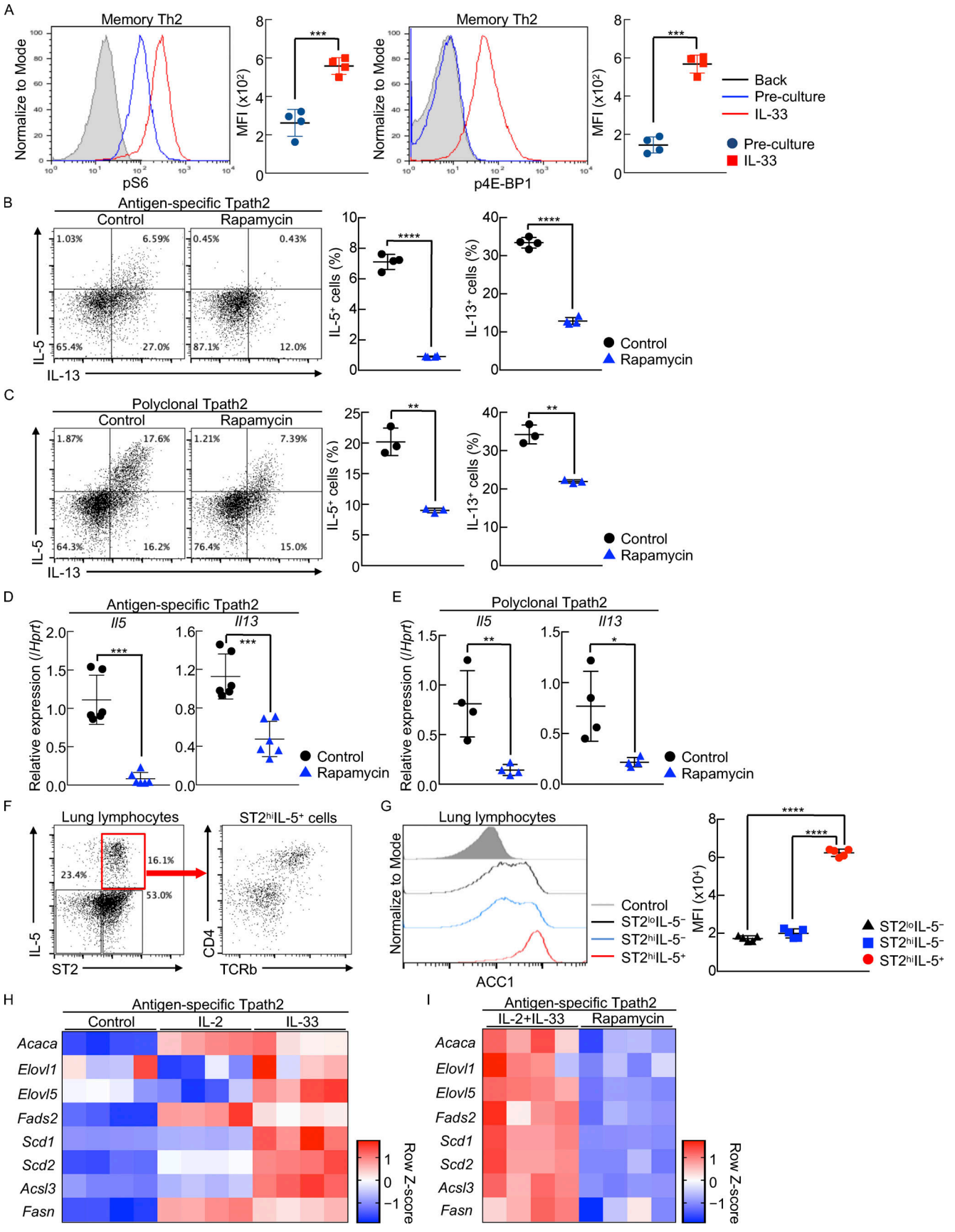


Figure 1. **ST2$^{hi}$ IL-5–producing Tpath2 cells express high levels of ACC1. (A)** p4E-BP1 and pS6 in memory Th2 cells were analyzed by FACS. MFI, mean fluorescence intensity. **(B and C)** Intracellular staining profiles of IL-5 and IL-13 in antigen-specific Tpath2 cells (B) or polyclonal Tpath2 cells (C) treated with or

without rapamycin (100 nM). **(D and E)** Quantitative RT-PCR analysis of *Il5* and *Il13* in antigen-specific Tpath2 cells (D) or polyclonal Tpath2 cells (E). **(F)** Representative intracellular staining profiles of IL-5 and ST2 in stimulated lung lymphocytes isolated from mice given IL-33 and expression of CD4 and TCRβ on the ST2$^{hi}$IL-5$^{+}$ population. **(G)** Expression of ACC1 in lung lymphocytes (three populations as shown in Fig. 1 F). **(H and I)** Heatmap visualization of expression profiles of genes involved in fatty acid biosynthesis in preculture, IL-2–cultured, and IL-33–cultured antigen-specific Tpath2 cells (H) or IL-2 plus IL-33–cultured antigen-specific Tpath2 cells treated with or without rapamycin (I). The Z-score scales ranging from blue to red are shown in the bottom right corner. For each group, $n$ = 4 (A–C, E, H, and I); $n$ = 5 (F and G); or $n$ = 6 (D) biologically independent samples are shown. More than three independent experiments were performed with similar results (A–I). Mean values with SD are shown (A–E and G). An unpaired two-tailed Student's $t$ test was applied for A–E and G. Statistical significance (P values) is indicated as *, P < 0.05; **, P < 0.01; ***, P < 0.001; ****, P < 0.0001.

### ACC1 controls the development of ST2$^{hi}$ IL-5–producing type 2 pathogenic lymphocytes

We next analyzed the involvement of ACC1 in the development of Tpath2 cells using the inducible ERT2-Cre–driven *Acaca*-deficient mouse system. Cultivation of ERT2-Cre$^{+}$*Acaca*$^{fl/fl}$ antigen-specific Tpath2 cells with 4-hydroxy tamoxifen (4-OHT) significantly reduced both protein and mRNA levels of IL-5 and IL-13 (Fig. 2, A and B). Similar to the findings in antigen-specific Tpath2 cells, IL-5 and IL-13 were also significantly reduced in ERT2-Cre$^{+}$*Acaca*$^{fl/fl}$ polyclonal Tpath2 cells cultured with 4-OHT (Fig. S2, A and B). IL-4 production was unaffected by the genetic deletion of *Acaca* in antigen-specific and polyclonal Tpath2 cells (Fig. S2, C and D; Endo et al., 2019). Similarly, treatment of antigen-specific or polyclonal Tpath2 cells with 5-(tetradecyloxy)-2-furoic acid (TOFA), a pharmacologic inhibitor of ACC1, substantially suppressed the production of IL-5 and IL-13 to levels similar to those in rapamycin-treated cells (Fig. 2, C and D; and Fig. S2, E and F).

We previously reported ST2 as a functional cell surface molecule of Tpath2 cells (Endo et al., 2015b). Consistent with the data of IL-5 and IL-13 production, the ST2 expression on antigen-specific and polyclonal Tpath2 cells was also suppressed by the genetic deletion or pharmacologic inhibition of ACC1 (Fig. 2, E–G; and Fig. S2, G and H). These results suggest that ACC1 is required for the differentiation of Tpath2 cells.

ILC2s and Tpath2 cells express several common factors of type 2 immune responses, including *Gata3*, *Il1rl1*, and *Icos* (Endo et al., 2014). Furthermore, Salmond et al. (2012) have reported that the activation of the mTOR signaling pathways by IL-33 is crucial for the effector function of ILC2s. As shown in Fig. 1 F, ST2$^{hi}$ IL-5–producing ILC2s expressed high levels of ACC1. Thus, we next assessed the role of ACC1 in the function of ILC2s. Similar to the findings in Tpath2 cells, TOFA and rapamycin treatment reduced the secretion of IL-5 and IL-13 from ILC2s (Fig. 2 H). Likewise, a significant reduction in *Il5* and *Il13* mRNA expression was detected by the pharmacologic inhibition of ACC1 in ILC2s (Fig. 2 I). The ST2 expression was also decreased by the inhibition of ACC1 (Fig. 2 J). These results indicate that ACC1 controls type 2 pathogenic innate and adaptive lymphocytes through the induction of ST2, IL-5, and IL-13.

### Genetic deletion of CD4$^{+}$ T cell–intrinsic ACC1 inhibits the Tpath2 cell responses and reduces airway inflammation in vivo

To assess the effect of the deletion of ACC1 on Tpath2 cells in vivo, we examined a papain-induced lung inflammation model using mice in which the biotin carboxyl carrier protein domain in the *Acaca* gene had been conditionally deleted in CD4$^{+}$ T cells, as illustrated in Fig. 3 A (Yamamoto et al., 2018). As shown in Fig. 3 B, ST2$^{hi}$ IL-5–producing Tpath2 cells in the lungs were decreased in the *Acaca*$^{-/-}$ group. We also assessed the bronchoalveolar lavage (BAL) fluid and found that the number of infiltrated cells and eosinophils in the BAL fluid was significantly decreased by the genetic deletion of *Acaca* in CD4$^{+}$ T cells (Fig. 3 C). In contrast, IL-5 production of CD44$^{hi}$CD4$^{-}$ cells, including ILC2s, was similar between the *Acaca*$^{+/+}$ and *Acaca*$^{-/-}$ groups (Fig. 3 D).

Papain is known to induce IL-33, IL-25, and thymic stromal lymphopoietin production by airway epithelial cells (Halim et al., 2014). Among them, IL-33 plays a critical role in the induction of IL-5–producing Tpath2 cells and ILC2s and the pathogenesis of eosinophilic airway inflammation (Endo et al., 2015b; Yamamoto et al., 2018). We therefore next directly administered IL-33 to the mice and assessed the role of ACC1 in the pathogenesis of asthma onset (Fig. 3 E). Similar to our findings in the papain-induced asthma model, IL-5–producing Tpath2 cells in the lung were reduced in the *Acaca*$^{-/-}$ group (Fig. 3 F). Furthermore, the number of eosinophils in the BAL fluids, infiltration of inflammatory cells in the lungs, mucus production, and mRNA levels of inflammatory markers for eosinophilic inflammation were also reduced in the *Acaca*$^{-/-}$ group (Fig. 3, G–J).

Next, *Acaca*$^{+/+}$ and *Acaca*$^{-/-}$ mice were intranasally challenged with OVA antigen after immunization with OVA/alum, and their ability to induce allergic airway inflammation was assessed (Fig. 4 A). Compared with the *Acaca*$^{+/+}$ group, the *Acaca*$^{-/-}$ group showed a significant decrease in the number of ST2$^{hi}$ IL-5–producing CD4$^{+}$ T cells in the lung and eosinophils in the BAL fluid, similar to results using the IL-33– or papain-induced lung inflammation models (Fig. 4, B and C). No obvious changes in numbers of the TCRβ$^{-}$CD4$^{-}$CD44$^{hi}$ST2$^{hi}$IL-5$^{+}$ population that contains ILC2s were observed between the two (Fig. 4 D). Histologic analysis also revealed a similar reduction in mononuclear cell infiltration into the peribronchiolar regions of the lungs (Fig. 4 E). Periodic acid–Schiff (PAS) staining and the measurement of *Gob5* or inflammatory markers in the lung tissues showed decreased production of mucus in the *Acaca*$^{-/-}$ group (Fig. 4, F and G). Notably, a significant reduction of total serum IgE and OVA-specific IgE in the *Acaca*$^{-/-}$ group was detected (Fig. 4, H and I). These results indicate that the genetic deletion of *Acaca* in CD4$^{+}$ T cells results in a reduction in ST2$^{hi}$ IL-5–producing Tpath2 cells and a decrease in eosinophilic inflammation in the lungs.

### ACC1 controls the production of common β cytokines, including IL-3 and GM-CSF, in memory Th2 cells

To further investigate the effect of ACC1 on cytokine production of CD4$^{+}$ T cells, we performed RNA-sequencing (RNA-seq)

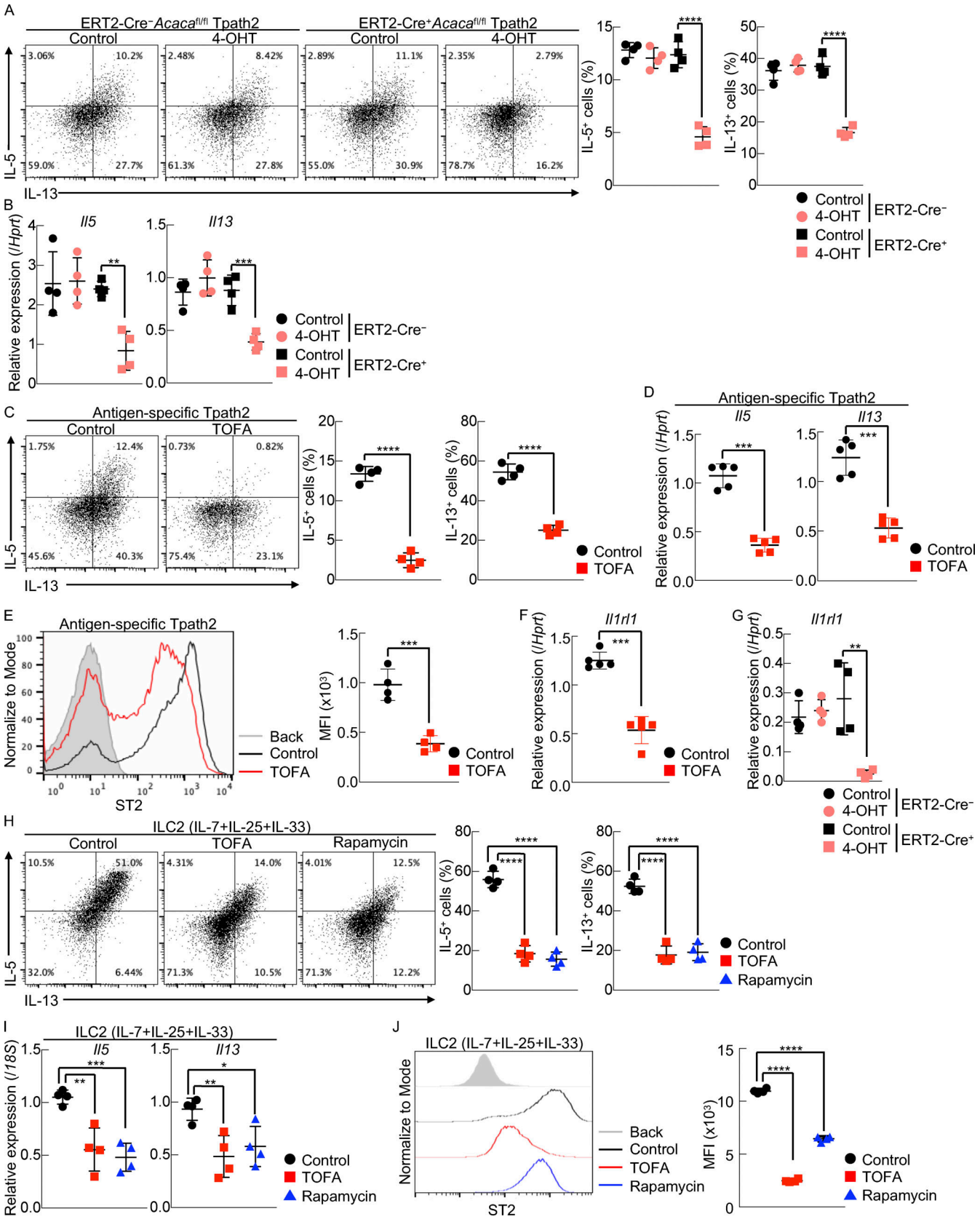


Figure 2. **ACC1 controls the development of ST2$^{hi}$ IL-5–producing pathogenic lymphocytes. (A)** Intracellular staining profiles of IL-5 and IL-13 in ERT2-Cre$^{-}$*Acaca*$^{fl/fl}$ or ERT2-Cre$^{+}$*Acaca*$^{fl/fl}$ Tpath2 cells treated with or without 4-OHT (100 nM). **(B)** Quantitative RT-PCR analysis of *Il5* and *Il13* in ERT2-Cre$^{-}$*Acaca*$^{fl/fl}$ or ERT2-Cre$^{+}$*Acaca*$^{fl/fl}$ Tpath2 cells cultured as in A. **(C)** Intracellular staining profiles of IL-5 and IL-13 in antigen-specific Tpath2 cells treated with or without TOFA. **(D)** Quantitative RT-PCR analysis of *Il5* and *Il13* in antigen-specific Tpath2 cells cultured as in C. **(E)** Expression profiles of ST2 on antigen-specific Tpath2

cells treated with or without TOFA. **(F)** Quantitative RT-PCR analysis of *Il1rl1* in antigen-specific Tpath2 cells treated with or without TOFA. **(G)** Quantitative RT-PCR analysis of *Il1rl1* in ERT2-Cre$^{-}$*Acaca*$^{fl/fl}$ or ERT2-Cre$^{+}$*Acaca*$^{fl/fl}$ Tpath2 cells cultured as in A. **(H)** Intracellular staining profiles of IL-5 and IL-13 treated with TOFA or rapamycin. **(I)** Quantitative RT-PCR analysis of *Il5* and *Il13* in ILC2s treated with TOFA or rapamycin. **(J)** Expression profiles of ST2 on ILC2s treated with TOFA or rapamycin. The cells isolated from ERT2-Cre$^{-}$*Acaca*$^{fl/fl}$ or ERT2-Cre$^{+}$*Acaca*$^{fl/fl}$ mice were used for A, B, and G. For each group, $n$ = 4 (A–C, E, and G–J) or $n$ = 5 (D and F) biologically independent samples are shown. More than three independent experiments were performed with similar results (A–J). Mean values with SD are shown (A–J). An unpaired two-tailed Student's $t$ test was applied in A–J. Statistical significance (P values) is indicated as *, P < 0.05; **, P < 0.01; ***, P < 0.001; ****, P < 0.0001.

analyses using ERT2-Cre$^{+}$*Acaca*$^{fl/fl}$ Tpath2 cells. We found that the expression values (fragments per kilobase of transcript per million mapped reads [FPKM]) of *Il3* and *Csf2* were substantially decreased in ACC1-deficient Tpath2 cells, as well as those of *Il5* and *Il13* (Fig. 5 A and Fig. S3 A). Expression of *Il4* was not affected by the genetic deletion of ACC1, as in Fig. S2 C. These data suggested that common β cytokines, including *Il5*, *Il3*, and *csf2*, were controlled in the same way by ACC1 in Tpath2 cells. As reported previously, the FPKM of *Il17a* and *Il17f* was also decreased in the *Acaca*$^{-/-}$ group, although the magnitude was substantially lower (Fig. S3 B; Endo et al., 2015a). Levels of other cytokines, such as *Ifng*, *Il6*, *Il24*, *Il1a*, *Il1b*, *Il16*, *Il21*, and *Il22*, were equivalent between *Acaca*$^{+/+}$ and *Acaca*$^{-/-}$ Tpath2 cells (Fig. 5 A and Fig. S3 B). We next confirmed the mRNA expression of *Il3* and *Csf2* in *Acaca*$^{-/-}$ Tpath2 cells, and a similar trend to the RNA-seq analyses was detected (Fig. 5 B). Similarly, TOFA treatment significantly reduced the expression of *Il3* and *Csf2* in Tpath2 cells (Fig. 5 C). Furthermore, we also detected a reduction in IL-3 and GM-CSF production by *Acaca*$^{-/-}$ or TOFA-treated Tpath2 cells (Fig. 5 D and Fig. S3 C). In addition, we observed a reduction in IL-3 and GM-CSF production by CD44$^{hi}$CD4$^{+}$ T cells in inflamed lungs collected from papain-treated mice (Fig. 5 E). These results suggest that ACC1 controls common β cytokines, including IL-5, IL-3, and GM-CSF, in Tpath2 cells.

### CD4$^{+}$ T cell–intrinsic ACC1 controls MC903-induced skin inflammation via IL-3–mediated basophil activation

The pathogenesis of AD involves interaction between Th2 cells, ILC2s, and basophils (Ito et al., 2011; Leyva-Castillo et al., 2013; Siracusa et al., 2013). Although IL-3 derived from activated CD4$^{+}$ T cells is essential for basophil activation in the pathology of AD, the cell-intrinsic factors regulating IL-3–producing T cells remain poorly understood (Leyva-Castillo et al., 2013). We therefore used a mouse model of calcipotriol (MC903)-induced AD to investigate whether CD4$^{+}$ T cell–intrinsic ACC1 influences skin inflammation (Fig. S4 A). In addition to the high expression of ACC1 in IL-5–producing Th2 cells in the lung, we found that IL-3–producing CD4$^{+}$ T cells express slightly higher levels of ACC1 than non–IL-3–producing cells in inflamed skin and draining lymph nodes (dLNs; Fig. 6 A and Fig. S4 B). Furthermore, a significant reduction in IL-3–producing CD4$^{+}$ T cells in the skin and dLNs was detected in MC903-treated *Acaca*$^{-/-}$ mice (Fig. 6 B and Fig. S4 C). The proportion of CD44$^{hi}$CD4$^{+}$ T cells in the skin was also decreased in the *Acaca*$^{-/-}$ group (Fig. S4 D). In contrast, IL-5–producing CD4$^{+}$ T cells in the skin and dLNs were rarely observed (Fig. S4, E and F). Consistent with these results, we found that the *Acaca*$^{-/-}$ group showed reduced swelling, reddening, and scaling of the ears compared with the *Acaca*$^{+/+}$ group (Fig. 6, C and D). In addition, a histological examination of the skin showed improved hyperkeratosis and epidermal hyperplasia following the genetic deletion of CD4$^{+}$ T cell–intrinsic ACC1 (Fig. 6 E). The difference in the clinical scores between groups reflected a reduction in inflammation in the *Acaca*$^{-/-}$ group (Fig. 6 F).

To determine whether IL-3 produced from ACC1-expressing CD4$^{+}$ T cells in the skin was functionally relevant to basophil activation, we next analyzed the phenotype of basophils that had infiltrated into inflamed skin. Although the number of basophils in the ear skin was similar between *Acaca*$^{+/+}$ and *Acaca*$^{-/-}$ mice (Fig. S4 G), the cell surface expression of CD63, an activation marker of basophils, was substantially reduced in *Acaca*$^{-/-}$ mice (Fig. 6 G). Thus, we postulated that ameliorated MC903-induced skin inflammation in *Acaca*$^{-/-}$ mice was caused by the suppression of IL-3–mediated basophil activation. We therefore next assessed whether IL-3 administration restored the phenotype of skin inflammation and basophil activation in MC903-treated *Acaca*$^{-/-}$ mice (Fig. S4 H). Since the biological half-life of IL-3 is very short, we used a mixture of IL-3 and anti-IL-3 to prolong the half-life and enhance the biological effects in vivo (Finkelman et al., 1993; Ohmori et al., 2009). As expected, IL-3 injection into *Acaca*$^{-/-}$ mice restored the phenotype, including the gross pathological findings and the histopathologic assessment of skin inflammation, to that in the *Acaca*$^{+/+}$ mice (Fig. 6, H and I). Similarly, the ear thickness and clinical score in the IL-3–treated *Acaca*$^{-/-}$ mice were also improved (Fig. 6, J and K), and CD63 expression on basophils in the *Acaca*$^{-/-}$ mice was increased to the same extent as in the *Acaca*$^{+/+}$ mice by IL-3 injection (Fig. 6 L). The expression of CD203c, a basophil-specific activation marker, was also augmented by the injection of IL-3 into *Acaca*$^{-/-}$ mice (Fig. 6 M). In contrast, the IL-3 production of CD44$^{hi}$CD4$^{+}$ T cells in dLNs was not affected by IL-3 injection (Fig. S4 I). These results suggest that CD4$^{+}$ T cell–intrinsic ACC1 controls MC903-induced skin inflammation via IL-3–mediated basophil activation.

### Pharmacologic deletion or inhibition of ACC1 by topical treatment attenuates MC903-induced skin inflammation

Next, to evaluate the effect of ACC1 on AD more accurately, we topically treated ERT2-Cre$^{+}$*Acaca*$^{fl/fl}$ mice with 4-OHT and selectively deleted the *Acaca* gene from skin lesions (Fig. 7 A). Topical 4-OHT treatment resulted in a significant reduction in IL-3–producing CD4$^{+}$ T cells in the skin though partial genetic deletion of *Acaca* in ear CD45$^{+}$ cells (Fig. 7 B and Fig. S4 J). Consistent with the findings in *Acaca*$^{-/-}$ mice, the ear thickness, swelling, and reddening were ameliorated in the ERT2-Cre$^{+}$*Acaca*$^{fl/fl}$ group compared with the ERT2-Cre$^{-}$*Acaca*$^{fl/fl}$ group (Fig. 7, C and D). Similarly, histological analysis and clinical scoring showed a reduction in hyperkeratosis and

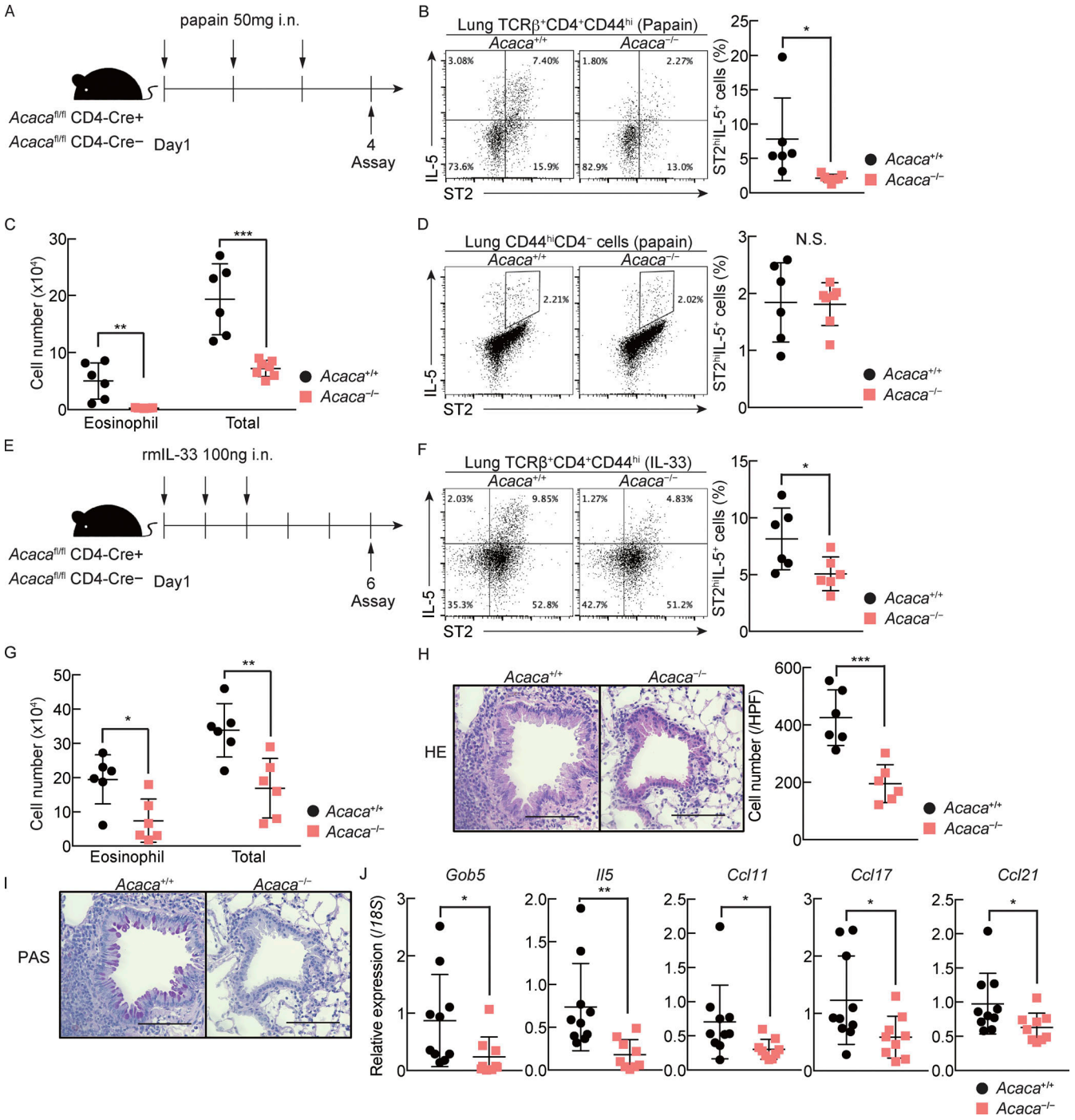


Figure 3. **Genetic deletion of CD4⁺ T cell–intrinsic ACC1 restrains Tpath2 cell responses and reduces airway inflammation in vivo. (A)** Experimental protocol for papain-induced lung inflammation model. **(B)** Intracellular staining profiles of ST2 and IL-5 in lung TCRβ⁺CD4⁺CD44$^{hi}$ cells. The percentage of ST2$^{hi}$IL-5⁺ cells is shown. **(C)** The absolute cell number of eosinophils and total cells in the BAL fluid collected from *Acaca*$^{+/+}$ or *Acaca*$^{-/-}$ mice intranasally administered with papain. **(D)** Intracellular staining profiles of ST2 and IL-5 in lung CD44$^{hi}$CD4$^{-}$ cells isolated from *Acaca*$^{+/+}$ or *Acaca*$^{-/-}$ mice. **(E)** Experimental protocol for IL-33–induced lung inflammation model. **(F)** Intracellular staining profiles of ST2 and IL-5 in stimulated lung TCRβ⁺CD4⁺CD44$^{hi}$ cells. The percentage of ST2$^{hi}$IL-5⁺ cells is shown. **(G)** The absolute cell number of eosinophils and total cells in the BAL fluid collected from *Acaca*$^{+/+}$ or *Acaca*$^{-/-}$ mice intranasally administered with IL-33. **(H)** Lung tissue sections of mice administered with IL-33 were fixed and stained with H&E (HE). A representative staining pattern is shown. Scale bars in bottom right corner represent 100 µm. Number of infiltrated inflammatory cells in lung per high power field (HPF) is shown. **(I)** Lung tissue sections of mice administered with IL-33 were fixed and stained with PAS. A representative staining pattern is shown. Scale bars in bottom right corner represent 100 µm. **(J)** Quantitative RT-PCR analysis of *Gob5*, *Il5*, *Ccl11*, *Ccl17*, and *Ccl21* in the lung tissues of *Acaca*$^{+/+}$ or *Acaca*$^{-/-}$ mice intranasally administered with IL-33. For each group, $n$ = 6–7 (B–D and F–H) or $n$ = 9–10 (J) biologically independent samples are shown. More than three independent experiments were performed with similar results (B–D and F–J). Mean values with SD are shown for B–D, F–H, and J. An unpaired two-tailed Student's $t$ test was applied for B–D, F–H, and J. Statistical significance (P values) is indicated as *, P < 0.05; **, P < 0.01; ***, P < 0.001.

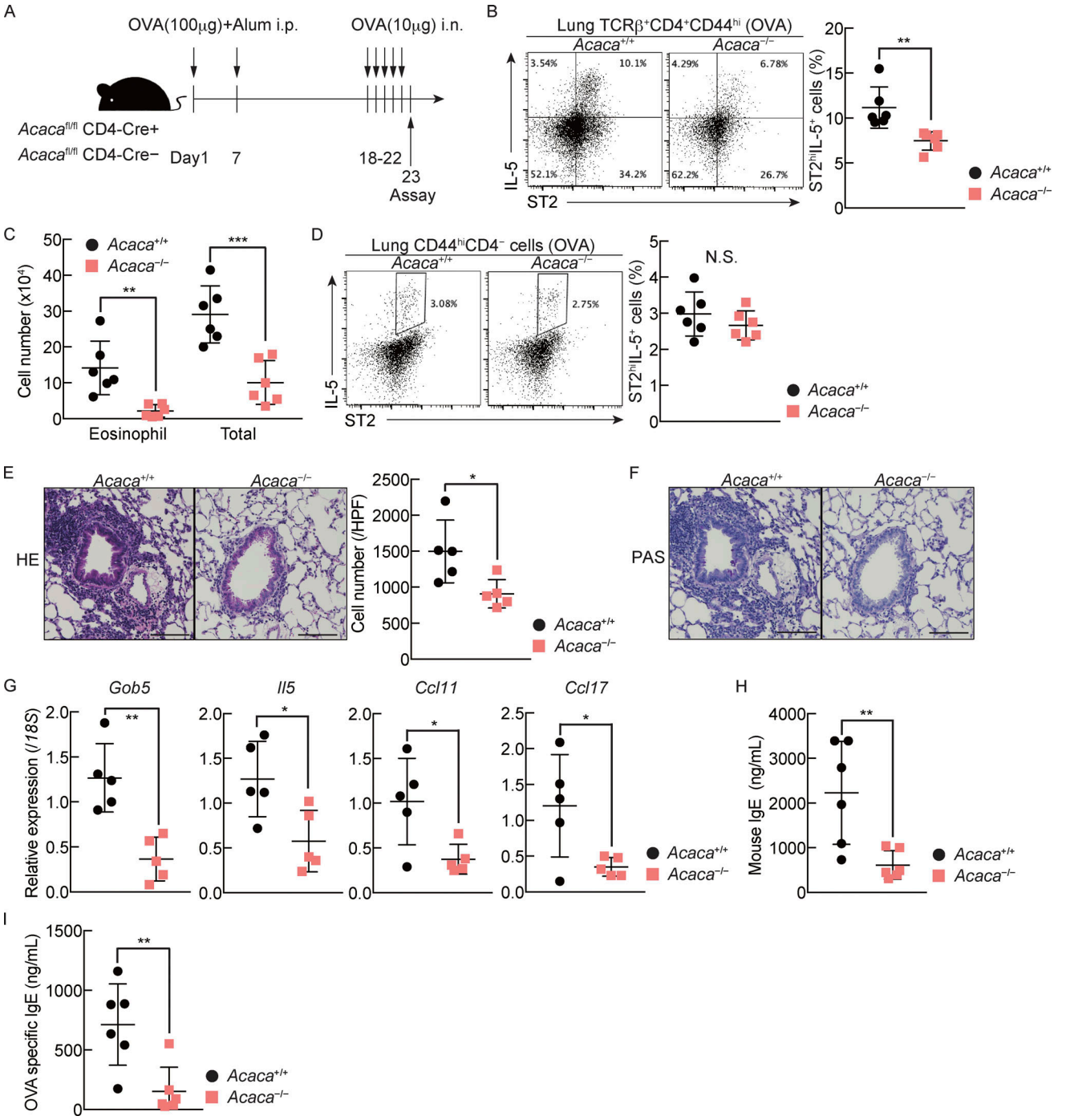


Figure 4. **Genetic deletion of CD4⁺ T cell–intrinsic ACC1 reduces lung allergic inflammation in vivo. (A)** Experimental protocol for OVA-induced lung inflammation model. **(B)** Intracellular staining profiles of ST2 and IL-5 lung TCRβ⁺CD4⁺CD44$^{hi}$ cells. The percentage of ST2$^{hi}$IL-5⁺ cells is shown. **(C)** The absolute cell number of eosinophils and total cells in the BAL fluid collected from *Acaca*$^{+/+}$ or *Acaca*$^{-/-}$ mice intranasally administered with OVA as in A. **(D)** Intracellular staining profiles of ST2 and IL-5 in lung CD44$^{hi}$CD4$^{-}$ cells isolated from *Acaca*$^{+/+}$ or *Acaca*$^{-/-}$ mice. **(E)** Lung tissue sections of mice administered with OVA were fixed and stained with H&E (HE). A representative staining pattern is shown. Scale bars in bottom right corner represent 100 µm. Number of infiltrated inflammatory cells in lung per high power field (HPF) is shown. **(F)** Lung tissue sections of mice administered with OVA were fixed and stained with PAS. A representative staining pattern is shown. Scale bars in bottom right corner represent 100 µm. **(G)** Quantitative RT-PCR analysis of *Gob5*, *Il5*, *Ccl11*, and *Ccl17* in the lung tissues of *Acaca*$^{+/+}$ or *Acaca*$^{-/-}$ mice intranasally administered with OVA. **(H and I)** Total serum IgE (H) or OVA-specific IgE (I) was tested using ELISA. For each group, $n$ = 6 (B–D, H, and I) or $n$ = 5 (E–G) biologically independent samples are shown. More than three independent experiments were performed with similar results for B–I. Mean values with SD are shown for B–E and G–I. An unpaired two-tailed Student's $t$ test was applied for B–E and G–I. Statistical significance (P values) is indicated as *, P < 0.05; **, P < 0.01; ***, P < 0.001.

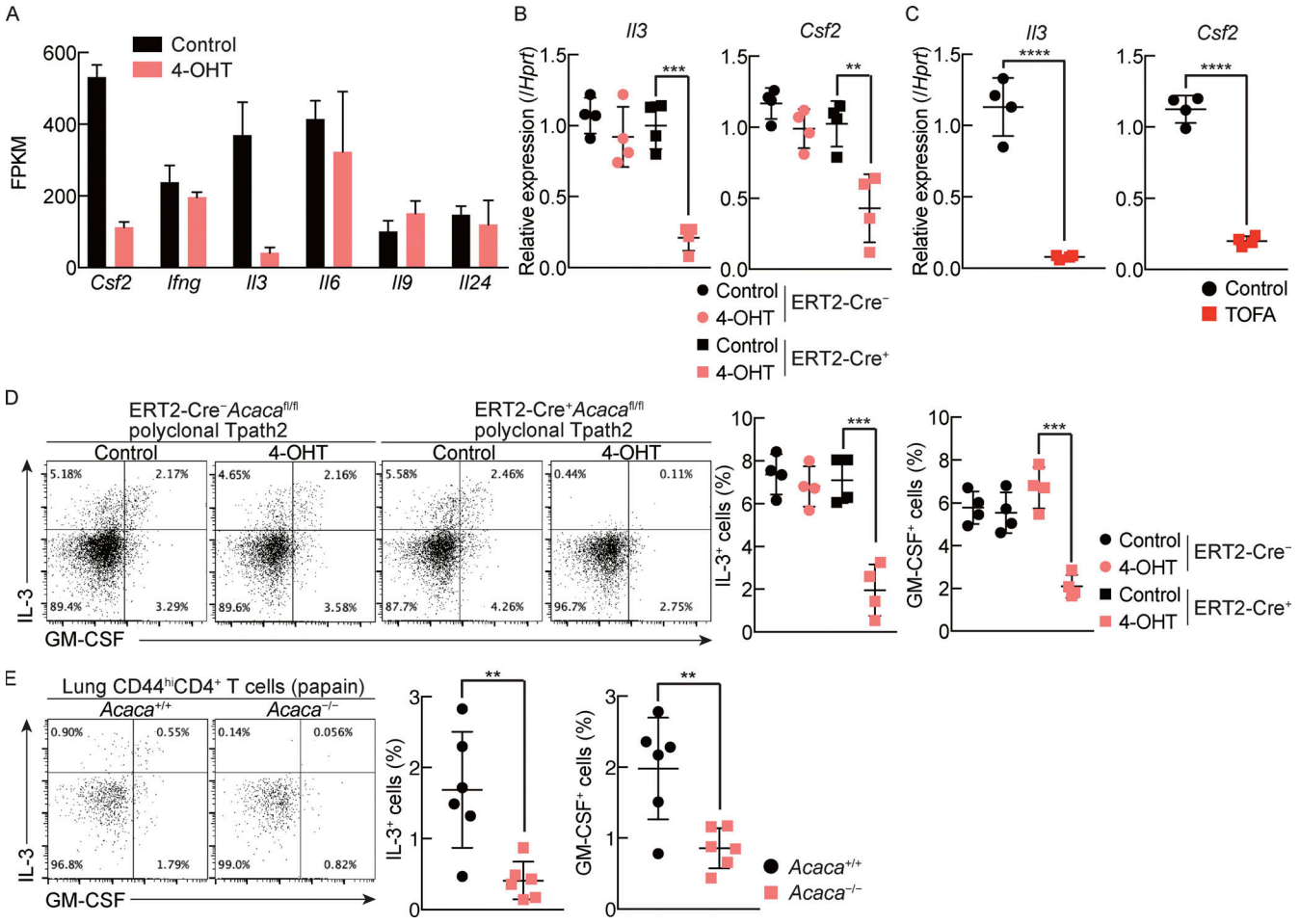


Figure 5. **ACC1 controls the production of common β cytokines, including IL-3 and GM-CSF, in memory Th2 cells. (A)** Expression profile by RNA-seq of selected cytokine genes in IL-33–cultured ERT2-Cre⁺*Acaca*$^{fl/fl}$ Tpath2 cells treated with or without 4-OHT. **(B)** Quantitative RT-PCR analysis of *Il3* and *Csf2* in IL-33–cultured ERT2-Cre⁻*Acaca*$^{fl/fl}$ or ERT2-Cre⁺*Acaca*$^{fl/fl}$ Tpath2 cells treated with or without 4-OHT. **(C)** Quantitative RT-PCR analysis of *Il3* and *Csf2* in IL-33–cultured antigen-specific Tpath2 cells treated with or without TOFA. **(D)** Intracellular staining profiles of IL-3 and GM-CSF in stimulated ERT2-Cre⁻*Acaca*$^{fl/fl}$ or ERT2-Cre⁺*Acaca*$^{fl/fl}$ polyclonal Tpath2 cells treated with or without 4-OHT. **(E)** Intracellular staining profiles of IL-3 and GM-CSF in stimulated lung CD44$^{hi}$CD4⁺ T cells. The cells were collected from *Acaca*$^{+/+}$ or *Acaca*$^{-/-}$ mice intranasally administered with papain. For each group, $n = 2$ (A); $n = 4$ (B–D); or $n = 6$ (E) biologically independent samples are shown. More than three independent experiments were performed with similar results for B–E. Mean values with SD are shown for B–E. An unpaired two-tailed Student's *t* test was applied for B–E. Statistical significance (P values) is indicated as **, $P < 0.01$; ***, $P < 0.001$; ****, $P < 0.0001$.

epidermal hyperplasia in the ERT2-Cre⁺*Acaca*$^{fl/fl}$ group (Fig. 7, E and F).

Furthermore, topical treatment with rapamycin or the ACC1 inhibitor CP-640186 hydrochloride in the MC903-induced skin inflammation model strongly reduced MC903-induced swelling, reddening, and scaling of the ears and clinical scoring (Fig. 7, G–J). These inhibitors also suppressed IL-3 production by CD44$^{hi}$CD4⁺ T cells in ear skin to a degree similar to that detected in *Acaca*$^{-/-}$ mice (Fig. 7 K). These results suggest that topical treatment of ACC1 inhibitor may have potential as a new therapeutic target for AD.

### ACC1-dependent de novo fatty acid biosynthesis together with maximal glycolytic capacity controls IL-5–producing Tpath2 cells

The metabolic transition toward increased aerobic glycolysis and anabolic pathways in activated T cells represents general metabolic reprogramming during rapid T cell activation and proliferation (Slack et al., 2015). We previously showed that anabolic fatty acid metabolism plays an essential role in antigen stimulation–dependent metabolic reprogramming of memory CD4⁺ T cells (Angela et al., 2016). To investigate the effect of ACC1 deficiency on the metabolic state of IL-5–producing Tpath2 cells, we analyzed the mitochondrial function and rate of acid efflux in *Acaca*-deficient or TOFA-treated Tpath2 cells by monitoring the oxygen consumption rate (OCR; indicator of oxidative phosphorylation) and extracellular acidification rate (ECAR; indicator of glycolysis) with an extracellular efflux analyzer. Sequential treatment with the ATPase inhibitor oligomycin, the uncoupling agent carbonyl cyanide 4-(trifluoromethoxy) phenylhydrazone, and the electron transport chain inhibitors rotenone and antimycin A revealed the basal oxygen consumption, ATP turnover, maximum respiratory capacity, and spare respiratory capacity (van der Windt et al., 2016). We found that the

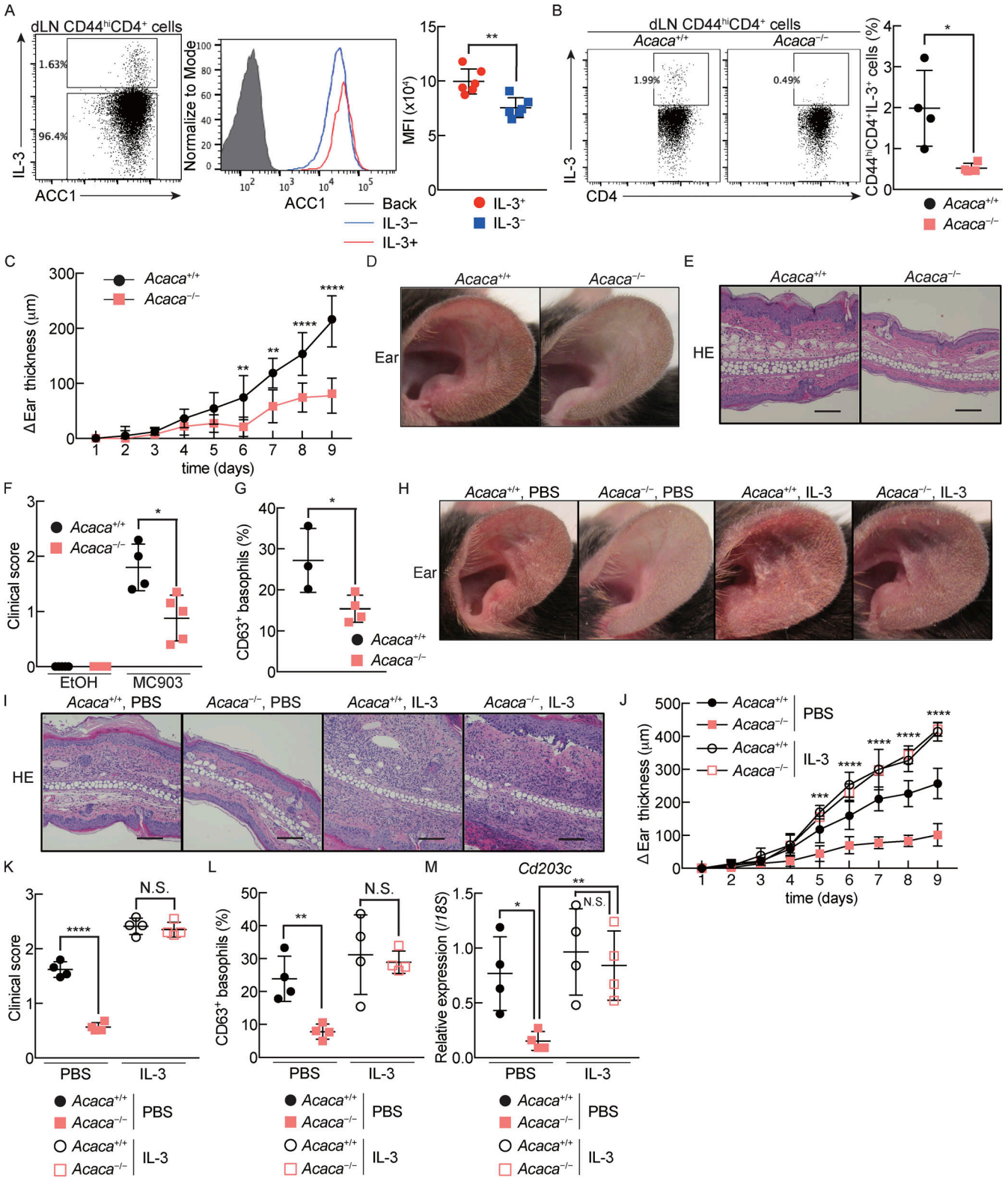


Figure 6. **ACC1 controls MC903-induced skin inflammation via IL-3–mediated basophil activation. (A)** Intracellular staining profiles of IL-3 and ACC1 in stimulated ear-dLN CD44$^{hi}$CD4$^{+}$ T cells. Histogram shows ACC1 expression in IL-3$^{+}$ or IL-3$^{-}$ cells. **(B)** Intracellular staining profiles of IL-3 in stimulated ear-dLN CD44$^{hi}$CD4$^{+}$ T cells. **(C)** Ear thickness of *Acaca*$^{+/+}$ and *Acaca*$^{-/-}$ mice after daily MC903 treatment (2 nmol per ear). Values are differences in thickness from day 0. **(D and E)** Representative images of ears collected from *Acaca*$^{+/+}$ or *Acaca*$^{-/-}$ mice topically treated with MC903 (D) and histological analysis of ear sections fixed and stained with H&E (HE; E). Scale bars represent 100 µm. **(F)** Clinical score of the ear skin based on the redness and swelling. **(G)** Expression of CD63 on ear-dLN basophils (CD45$^{int}$CD200R3$^{+}$CD49b$^{+}$c-kit$^{-}$) of *Acaca*$^{+/+}$ or *Acaca*$^{-/-}$ mice. **(H and I)** Representative images of ears collected from *Acaca*$^{+/+}$ and *Acaca*$^{-/-}$ mice subcutaneously administered with mIL-3/anti-IL-3 or PBS to shoulders (H). Histological analysis of ear sections of mice fixed and stained with H&E (I).

Scale bars represent 100 µm. **(J)** Ear thickness of *Acaca*$^{+/+}$ and *Acaca*$^{-/-}$ mice subcutaneously injected with mIL-3/anti-IL-3 mixture or PBS, after daily MC903 treatment. Values are differences in thickness from day 0. P values indicated comparison with *Acaca*$^{+/+}$ group administered PBS and *Acaca*$^{+/+}$ or *Acaca*$^{-/-}$ group administered IL-3 mixture. **(K)** Clinical score of the ear skin based on redness and swelling. **(L)** Expression of CD63 on ear-dLN basophils (CD45$^{int}$CD200R3$^{+}$CD49b$^{+}$c-kit$^{-}$) of *Acaca*$^{+/+}$ and *Acaca*$^{-/-}$ mice subcutaneously injected with mIL-3/anti-IL-3 or PBS, after daily MC903 treatment. **(M)** Quantitative RT-PCR analysis of *Cd203c* in tissue section of ear, same condition as in L. For each group, $n = 4$ (B–E and J–M); $n = 6$ (A); $n = 3$–4 (G); or $n = 4$–5 (F) biologically independent samples are shown. More than three independent experiments were performed with similar results for A–M. Mean values with SD are shown for A–C, F–G, and J–M. Two-way ANOVA was applied for C and J. An unpaired two-tailed Student's *t* test was applied for A, B, F, G, and K–M. Statistical significance (P values) is indicated as *, P < 0.05; **, P < 0.01; ***, P < 0.001; ****, P < 0.0001; N.S., not significant.

OCR and ECAR were lower in ACC1-deficient or TOFA-treated Tpath2 cells than in control cells (Fig. 8, A–D). These results indicate that ACC1-induced de novo fatty acid biosynthesis is required for the induction of metabolic reprogramming in Tpath2 cells.

We previously reported that extrinsic fatty acid supplementation restored the function of *Acaca*$^{-/-}$ Th17 cells and improved the proliferation, survival, and metabolic reprogramming of TOFA-treated activated CD4$^{+}$ T cells (Angela et al., 2016; Endo et al., 2015a). We therefore next analyzed whether extrinsic fatty acid supplementation restored the function and cell proliferation of TOFA-treated Tpath2 cells. We found that extrinsic supplementation of TOFA-treated Tpath2 cells with oleic acid (OA) partially restored cell numbers (Fig. 8 E). Furthermore, extrinsic supplementation of TOFA-treated Tpath2 cells with OA restored OCR to levels nearly equivalent to those in control cells (Fig. 8 F). In contrast, intermediate restoration was observed for ECAR by the supplementation of TOFA-treated Tpath2 cells with OA (Fig. 8 G). Unexpectedly, IL-5 production by TOFA-treated polyclonal Tpath2 cells was not restored at all by OA supplementation alone (Fig. 8 H). We speculated that maximal activation of the glycolysis pathway is required for IL-5 production by Tpath2 cells. To address this, we added extra glucose to OA-treated Tpath2 cell cultures and assessed IL-5 production. As shown in Fig. 8 I, glucose supplementation together with OA dramatically restored IL-5 production by TOFA-treated Tpath2 cells. A similar trend was detected in the mRNA expression of *Il5* (Fig. 8 J). These results suggest that de novo fatty acid biosynthesis together with maximal glycolytic capacity is essential for IL-5 production by Tpath2 cells.

### Acetate promotes chromatin accessibility at the *Il3* locus in *Acaca*$^{-/-}$ Th2 cells

We also evaluated the effect of extra glucose supplementation on IL-3 production by Th2 cells, but no significant changes were observed (Fig. S5 A). The short-chain fatty acid acetate is known to be an alternative carbon source for cancer cells or T cells, supporting their survival, proliferation, and function under nutrient-limited conditions (Comerford et al., 2014; Qiu et al., 2019). Furthermore, supplementation of acetate has been shown to enhance *Ifng* gene transcription in CD8$^{+}$ T cells via the promotion of histone acetylation and chromatin accessibility (Qiu et al., 2019; Vodnala et al., 2019). To investigate whether the restriction of fatty acid biosynthesis in CD4$^{+}$ T cells decreases the availability of cellular Ac-CoA for histone acetylation, we assessed global histone acetylation in TOFA-treated Th2 cells by Western blotting. We found that the acetylation of histone protein H3 was decreased in TOFA-treated Th2 cells compared with control cells (Fig. 9 A). We therefore further assessed the effects of supplemental acetate on IL-3 production by TOFA-treated or *Acaca*$^{-/-}$ Th2 cells. As expected, supplementation of acetate to TOFA-treated or *Acaca*$^{-/-}$ Th2 cell cultures restored the generation of IL-3–producing cells (Fig. 9, B and C). The gene expression of *Il3* was also up-regulated by the supplementation of TOFA-treated or *Acaca*$^{-/-}$ Th2 cells with acetate (Fig. 9, D and E). To determine whether acetate enhances the production of IL-3 by TOFA-treated Th2 cells by promoting histone acetylation and supporting gene transcription, we assessed histone acetylation by performing a chromatin immunoprecipitation (ChIP) assay. We found that acetate supplementation increased H3K9 acetylation at the *Il3* promoter region, where clusters are defined by similarity of DNase I–hypersensitivity site profiles (Duncliffe et al., 1997; Fig. 9 F and Fig. S5 B). To evaluate the importance of histone acetylation on IL-3 production more detail, we next analyzed whether administration of a histone acetyl transferase (HAT) inhibitor suppresses IL-3 production of Th2 cells. As shown in Fig. S5 C, the potent HAT inhibitor Curcumin suppressed IL-3 production by Th2 cells. We also assessed whether histone deacetylase (HDAC) inhibitors could enhance IL-3 production. Treatment of Th2 cells with trichostatin A (TSA), which is an organic compound that selectively inhibits the class I and II HDAC families of enzymes, enhanced IL-3 production (Fig. S5 D). These results suggest that histone acetylation is essential for the expression of *Il3* by Th2 cells.

Given the above findings, we propose that selective ACC1 expression and active fatty acid biosynthesis can be new hallmarks of cellular metabolism characterizing Tpath2 cells that facilitate granulocyte activation–dependent allergic inflammation (Fig. 9 G and Fig. S5 E).

## Discussion

Pathogenic CD4$^{+}$ T cell populations drive chronic inflammatory disorders in response to cell-extrinsic environmental factors, such as alarmins and cytokines (Saravia et al., 2019; Walker and McKenzie, 2018). However, the cell-intrinsic metabolic pathways that control pathogenic CD4$^{+}$ T cell function are unclear. We found that ACC1-dependent fatty acid biosynthesis plays a crucial role in Tpath2 cell differentiation and the pathogenesis of type 2 inflammation in the lung and skin. Furthermore, CD4$^{+}$ T cell–intrinsic ACC1 deletion attenuated allergic responses during eosinophilic and basophilic inflammation. Mechanistically, mTORC1-ACC1 orchestrated cell metabolism, fatty acid biosynthesis, and maximal activation of glycolysis to facilitate IL-5 production by Tpath2 cells. In addition, we found that IL-3 production was controlled by an epigenetic mechanism, as

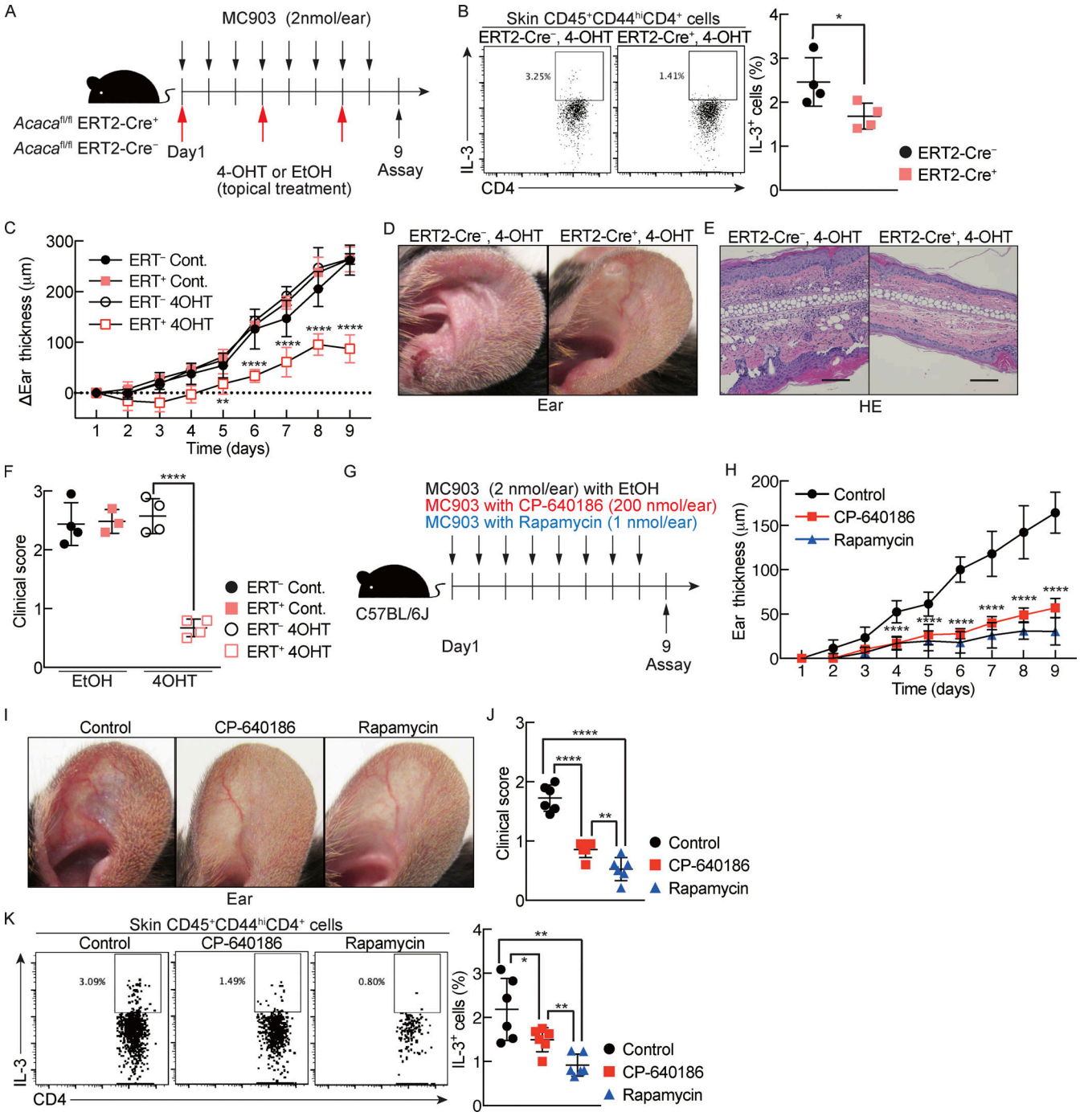


Figure 7. **ACC1 deletion or inhibition to whole cells in ear region by topical treatment of 4-OHT or inhibitors reduces MC903-induced skin inflammation. (A)** Experimental protocol for MC903-induced skin inflammation model with ERT2-Cre$^{-}$*Acaca*$^{fl/fl}$ or ERT-Cre$^{+}$*Acaca*$^{fl/fl}$ mice. **(B)** Intracellular staining profiles of IL-3 in ear CD45$^{+}$CD44$^{hi}$CD4$^{+}$ T cells in 4-OHT–treated ERT-Cre$^{+}$*Acaca*$^{fl/fl}$ or ERT2-Cre$^{-}$ mice. **(C)** Ear thickness of ERT-Cre$^{+}$*Acaca*$^{fl/fl}$ or ERT-Cre$^{-}$ mice given 4-OHT or EtOH (vehicle) topically. Values are differences in thickness from day 0. Statistical significance indicates difference between ERT-Cre$^{+}$*Acaca*$^{fl/fl}$ with 4-OHT group and the others. Cont., control. **(D and E)** Representative images of ears of ERT-Cre$^{+}$*Acaca*$^{fl/fl}$ or ERT2-Cre$^{-}$ mice given 4-OHT topically (D). Ear tissue sections of mice were fixed and stained with H&E (E). Scale bars represent 100 µm. **(F)** Clinical score of ear redness and scaling. **(G)** Experimental protocol for MC903-induced skin inflammation model treated with rapamycin or CP-640186. **(H)** Ear thickness of mice treated topically with rapamycin or CP-640186 versus control mice. Values are differences in thickness from day 0. Statistical significance indicates difference between rapamycin or CP-640186 group and control. **(I)** Representative images of ears of rapamycin- or CP-640186–treated mice with control. **(J)** Clinical score of rapamycin- or CP-640186–treated mice with control, assessed by ear redness and scaling. **(K)** Intracellular staining profiles of IL-3 in ear CD45$^{+}$CD44$^{hi}$CD4$^{+}$ T cells in rapamycin- or CP-640186–treated mice. For each group, $n = 4$ (B–F) or $n = 6$ (H–K) biologically independent samples are shown. More than three independent experiments were performed with similar results for B–E and H–K. Mean values with SD are shown for B, C, F, H, J, and K. Two-way ANOVA was applied for C and H. An unpaired two-tailed Student's *t* test was applied for B, F, J, and K. Statistical significance (P values) is indicated as *, $P < 0.05$; **, $P < 0.01$; ****, $P < 0.0001$.

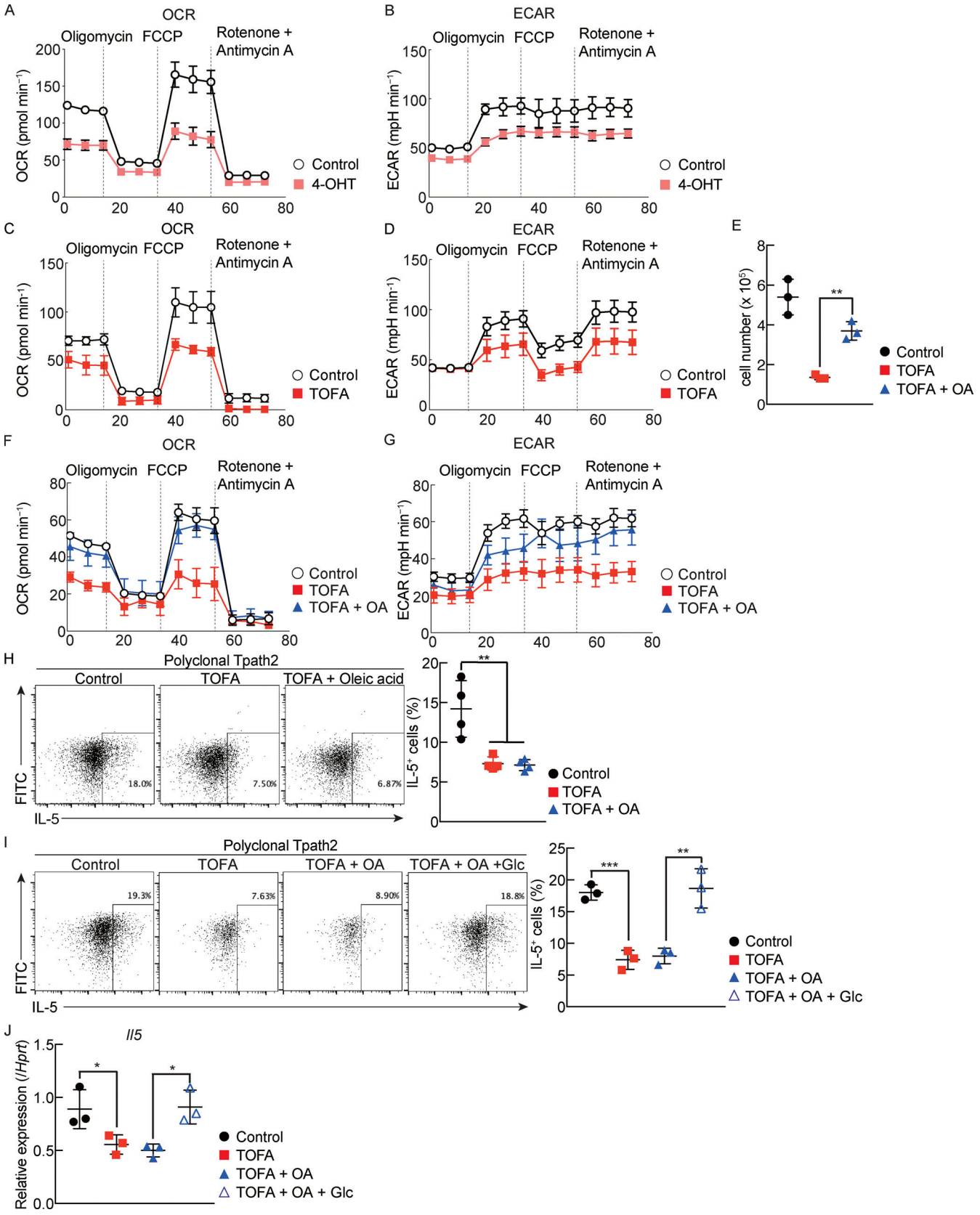


Figure 8. **ACC1-dependent de novo fatty acid biosynthesis together with maximal glycolytic capacity controls IL-5–producing Tpath2 cells. (A)** OCR of ERT2-Cre$^{+}$*Acaca*$^{fl/fl}$ Tpath2 cells treated with or without 4-OHT. FCCP, carbonyl cyanide 4-(trifluoromethoxy) phenylhydrazone. **(B)** ECAR of Tpath2 cells cultured as in A. **(C)** OCR of Tpath2 cells after 5-d cultivation with IL-33 plus TOFA or without TOFA. **(D)** ECAR of Tpath2 cells after 5-d cultivation with IL-33 plus TOFA or without TOFA. **(E)** The graph shows the number of Tpath2 cells after 5-d culture with TOFA in the presence or absence of OA (50 µM). **(F)** OCR of

Tpath2 cells treated with TOFA in the presence or absence of OA as in E. **(G)** ECAR of Tpath2 cells cultured as in F. **(H)** Intracellular staining profiles of IL-5 in polyclonal Tpath2 cells treated with TOFA or TOFA plus OA (50 µM). **(I)** Intracellular staining profiles of IL-5 in polyclonal Tpath2 cells treated with TOFA in the presence or absence of OA (50 µM) and glucose (50 mM). **(J)** Quantitative RT-PCR analysis of *Il5* in polyclonal Tpath2 cells cultured as in I. For each group, $n = 3$ (E–J); $n = 4$ (H); or $n = 5$–6 (A–D, F, and G) biologically independent samples are shown. The cells isolated from ERT-Cre$^{+}$*Acaca*$^{fl/fl}$ mice are used for A and B. More than three independent experiments were performed with similar results for A–J. Mean values with SD are shown for A–J. An unpaired two-tailed Student's *t* test was applied for E and H–J. Statistical significance (P values) is indicated as *, P < 0.05; **, P < 0.01; ***, P < 0.001.

evidenced by the fact that supplementation of acetate to *Acaca*$^{-/-}$ Th2 cell cultures restored histone acetylation at the *Il3* promoter region (Fig. S5 E). Taken together, our findings indicate that the ACC1-dependent fatty acid biosynthesis pathway serves as an essential metabolic checkpoint controlling Th2 cell pathogenicity and the development of allergic inflammation.

Raptor-mTORC1 signaling has been found to coordinate glycolysis and lipid biosynthesis to mediate TCR stimulation-induced exit from quiescence in Th2 cells (Yang et al., 2013). Another study reported that antigen-driven mTORC1/SREBP-mediated lipid metabolism plays a critical role in the activation and proliferation of CD8$^{+}$ T cells (Kidani et al., 2013). We now show that IL-33–induced mTORC1 activation is critical for the ACC1-mediated fatty acid biosynthesis and pathogenic function of Tpath2 cells. Consistent with our findings, IL-33 induces mTORC1 activation and phosphorylation of downstream effector proteins through ST2 signaling and the activation of phosphoinositide 3-kinase in ILC2s (Salmond et al., 2012). Of note, ACC1 expression in ST2$^{hi}$ IL-5–producing Tpath2 cells was selectively higher than in non–ST2$^{hi}$ IL-5-producing cell populations and ST2$^{lo}$ populations. This result indicates that mTORC1 activation differs between ST2$^{hi}$ IL-5–producing Tpath2 cells and non–ST2$^{hi}$ IL-5-producing cells. A possible explanation for this difference is that different glucose or amino acid availability controls the activation status of mTORC1 signaling in these populations (Jewell and Guan, 2013; Saxton and Sabatini, 2017). Indeed, glycolysis activity characterized by ECAR was lower in TOFA-treated and ACC1-deficient Tpath2 cells than in control cells. Furthermore, extrinsic glucose and OA supplementation to TOFA-treated Tpath2 cell cultures significantly restored IL-5 production. Previous findings suggest that cell-intrinsic Arginase 1 regulates proliferation and effector function of ILC2s via the control of maximal glycolytic capacity (Monticelli et al., 2016). Thus, the effector function, especially IL-5 production, in Tpath2 cells or ILC2s appears to be strictly regulated by an active metabolic circuit coordinated by mTORC1, ACC1-mediated fatty acid biosynthesis, and maximal glycolytic activity.

In contrast to IL-5, ACC1-dependent IL-3 production is controlled by epigenetic mechanisms. While transcriptional regulation of *Il3* is not well characterized, T cell–selective DNase I hypersensitivity sites at the *Il3* locus have been reported (Duncliffe et al., 1997). Our data highlight the role of acetate as an alternative carbon source for histone acetylation at the *Il3* promoter region in Th2 cells when synthesized fatty acids are limited. Acetate is known to enhance IFNγ production from CD8$^{+}$ T cells during prolonged glucose restriction (Qiu et al., 2019; Vodnala et al., 2019). Furthermore, acetate and butyrate can promote *Foxp3* expression to induce the differentiation of regulatory T cells in the gut (Furusawa et al., 2013). Thus, the gene group including *Il3*, *Csf2*, *Ifng*, and *Foxp3* appears to be favorably regulated by feeding of cellular Ac-CoA into histone proteins. Although the detailed mechanisms underlying how ACC1 controls the availability of cellular Ac-CoA for histone acetylation remain unclear, our previous data have shown that cellular Ac-CoA likely feeds into the cellular pool of metabolites in the tricarboxylic acid cycle in *Acaca*$^{-/-}$ Th1 and Th2 cells (Endo et al., 2019).

An intriguing finding in the present study is that ACC1-dependent fatty acid biosynthesis appears to control specific cytokines, including IL-5, IL-3, and GM-CSF, in CD4$^{+}$ T cells. In addition, we and other groups previously reported that IL-17A and IL-17F were impaired in *Acaca*$^{-/-}$ Th17 cells (Berod et al., 2014; Endo et al., 2015a). Among Th2 cytokines, IL-13 production is also partially decreased in *Acaca*$^{-/-}$ Tpath2 cells, whereas IL-4 is totally unaffected. RNA-seq analysis also revealed that other cytokines such as *Ifng*, *Il6*, *Il9*, and *Il24* were unchanged by genetic deletion of *Acaca* in Tpath2 cells. IL-5 and IL-3 play a crucial role in the pathogenesis of type 2 inflammation, and IL-17A and GM-CSF have a pathogenic role in a variety of autoimmune diseases (Broughton et al., 2012; Lotfi et al., 2019; Maddur et al., 2012). Therefore, we speculate that a high expression of ACC1 is a key hallmark of pathogenic cytokine production by T cells. In contrast to the selective effect of ACC1 inhibition on cytokine production, rapamycin-treated or mTOR-deficient CD4$^{+}$ T cells fail to differentiate into all Th1, Th2, or Th17 cells (Chi, 2012; Pollizzi and Powell, 2014). Furthermore, T cell–specific genetic deletion of Raptor, the scaffolding subunit of mTORC1, abrogates T cell priming, antigen-stimulated IL-2 production, and Th cell subset differentiation (Yang et al., 2013). These broad effects on T cell function by mTOR disruption make it reasonable to consider that mTOR is a critical regulator that integrates multiple inputs from environmental signals such as nutrients, growth factors, and cytokines.

In addition to our data suggesting the importance of fatty acid biosynthesis in Tpath2 cells and ILC2s, transient storage of fatty acids in lipid droplets was recently shown to regulate ILC2 responses in the lung (Karagiannis et al., 2020). That study showed esterification of fatty acids into triacylglycerols in ILC2s and that exogenous fatty acids are particularly important for mediating ILC2 proliferation (Karagiannis et al., 2020) Similarly, another report found that highly proliferating cells rely on external fatty acids to build complex lipids for cellular membranes (Yao et al., 2016). In conjunction with these reports, we previously reported that PPARγ-dependent fatty acid uptake programs are required for the rapid proliferation of activated CD4$^{+}$ T cells (Angela et al., 2016). However, supplementation of fatty acids was able to rescue the proliferation of Tpath2 cells. Therefore, both de novo fatty acid biosynthesis and the uptake of

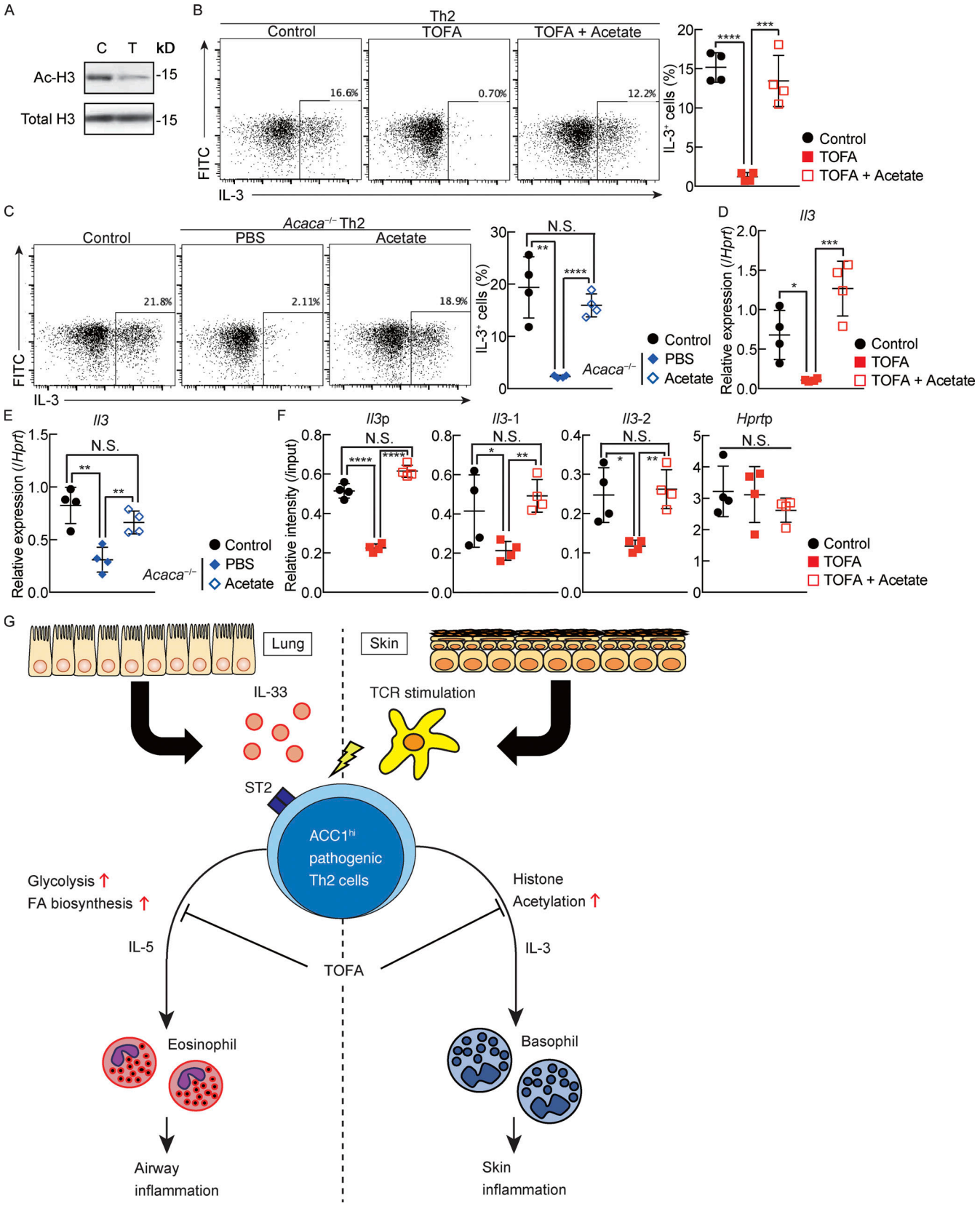


Figure 9. **Acetate promotes chromatin accessibility at the *Il3* locus in *Acaca*$^{-/-}$ Th2 cells. (A)** Western blot analysis of acetylated histone H3K9 and total histone H3 in Th2 cells treated with or without TOFA (C control; T, TOFA). **(B)** Intracellular staining profiles of IL-3 in restimulated Th2 cells treated with TOFA in the presence or absence of acetate (5 mM). **(C)** Intracellular staining profiles of IL-3 in restimulated *Acaca*$^{-/-}$ Th2 cells treated with acetate (5 mM). *Acaca*$^{-/-}$ Th2 cells were differentiated from CD4-Cre$^{+}$*Acaca*$^{fl/fl}$ mouse–derived naive CD4 T cells. **(D)** Quantitative RT-PCR analysis of *Il3* in Th2 cells cultured as in B.

**(E)** Quantitative RT-PCR analysis of *Il3* in *Acaca*$^{-/-}$ Th2 cells cultured as in C. **(F)** ChIP assays were performed with anti-acetyl histone H3-K9 at the *Il3* locus from Th2 cells. The intensities of these modifications relative to input DNA were determined by quantitative RT-PCR analysis. **(G)** Schematic diagram of ACC1$^{hi}$ Tpath2 cell–induced airway inflammation and skin inflammation. For each group, $n = 2$ (A) or $n = 4$ (B–F) biologically independent samples are shown. More than three independent experiments were performed with similar results for A–F. Mean values with SD are shown for B–F. An unpaired two-tailed Student's *t* test was applied for B–F. Statistical significance (P values) is indicated as *, P < 0.05; **, P < 0.01; ***, P < 0.001; ****, P < 0.0001; N.S., not significant.

extrinsic fatty acids are required for Tpath2 cells and ILC2s to meet their lipid demands.

In summary, we demonstrated that ACC1 controls the production of IL-5 and IL-3, which consequently determines the pathology of Th2 cells in the lung and skin, respectively. Thus, ACC1 and the de novo fatty acid biosynthesis pathway may be potential therapeutic targets for the treatment of type 2 inflammatory diseases, including asthma and AD.

## Materials and methods

### Mice

*Acaca*$^{fl/fl}$ mice (Mao et al., 2006) were crossed with CD4-Cre and ERT2-Cre mice (Jackson Laboratory) 10 times and maintained on a C57BL/6 background. OVA-specific TCR-αβ (DO11.10) transgenic mice were provided by Dr. D. Loh (Washington University School of Medicine, St. Louis, MO), and backcrossed to BALB/c mice 10 times (Murphy et al., 1990). C57BL/6, BALB/c, and BALB/c *nu/nu* mice were purchased from Clea. All mice were used at 6–10 wk of age and were housed under specific pathogen–free conditions. The animal experiments were performed with protocols approved by the Institutional Animal Care and Use Committee of Kazusa DNA Research Institute (registration no. 30-1-002). Experiments and animal care were performed according to the guidelines of Kazusa DNA Research Institute.

### Reagents

The reagents in this study are as follows: PE-conjugated anti-p4EBP1 (560285, clone M31-16), Alexa Fluor 647–conjugated anti-pS6 (560465, clone N5-676), PE/Cy7- and BV650-conjugated anti-CD4 (PE/Cy7; 552775, BV650; 563747, clone RM4-5), PE-conjugated anti-CD62L (553151, clone MEL-14), APC- and BV480-conjugated anti-CD44 (APC; 559250, BV480; 566200, clone IM7), BV421-conjugated anti-IL-4 (562915, clone 11B11), BV605-conjugated anti-TCRβ (562840, clone H57-597), and BV786-conjugated anti-CD45 (563754, clone 30-F11), all purchased from BD Biosciences.

PE- and BV421-conjugated anti-IL-33Rα (ST2; 145304, clone DIH9), APC-conjugated anti-CD200R3 (142207, clone Ba13), APC-conjugated anti-IL-5 (504306, clone TRFK5), APC-conjugated anti-IL-3 (503908, clone MP2-8F8), Alexa Fluor 488–conjugated anti-CD49b (103510, clone Hma2), APC-conjugated anti-IL-7Ra (135012, clone A7R34), PE/Cy7-conjugated anti-c-kit (105814, clone 2B8), PE/Cy7-conjugated anti-CD183 (CXCR3; 126516, clone CXCR3-173), FITC-conjugated anti-CD90.2 (140304, clone 53-2.1) and anti-GM-CSF (505404, clone MP1-22E9), PE-conjugated anti-CD63 (143904, clone NVG-2), FITC- and PE-conjugated anti-Lineage cocktail (FITC, 78022; PE, 78035; containing CD3, Gr-1, CD11b, B220, and Ter-119), and Zombie NIR fixable viability kit (423106) were purchased from BioLegend.

PE-conjugated anti-IL-13 (12–7133-82, clone eBio13A) was purchased from eBioscience. FITC-conjugated anti-TCRβ (35–5961-U100, clone H57-597) was purchased from Tonbo Biosciences. Alexa Fluor 488–conjugated anti-rabbit IgG fab2 (4412S) was purchased from Cell Signaling. Alexa Fluor 647–conjugated donkey anti-rabbit IgG (H+L) (A31573) was purchased from Invitrogen. Anti-acetyl coenzyme a carboxylase (109368) was purchased from Abcam. Recombinant murine IL-2 (212-12; Peprotech), IL-4 (214-14; Peprotech), IL-7 (217-17; Peprotech), IL-33 (580508; BioLegend), and IL-17E/IL-25 (1399-IL-025/CF; R&D Systems) were used for cell culture. TOFA and rapamycin purchased from Merck were used as pharmacologic inhibitors. 4-OHT purchased from Sigma-Aldrich was used for gene deletion with the inducible Cre/loxP estrogen receptor transgenic system. Curcumin (C7727; Sigma-Aldrich) was used as an HAT inhibitor. TSA (T8552; Sigma-Aldrich) was used as an HDAC inhibitor. CP-640186 hydrochloride (HY-15259A; MCE) was used as an ACC1 inhibitor.

### Cell preparation

For in vivo generation of polyclonal Tpath2 cells and ILC2s, recombinant mouse IL-33 (0.5 µg per mouse) was injected intraperitoneally into each mouse for five consecutive days, and CD44$^{hi}$CD4$^{+}$ T cells and ILC2s were isolated from the spleen. After presorting by autoMACS (Miltenyi Biotec), CD44$^{hi}$CD62L$^{lo}$ T cells (CD4$^{+}$TCRβ$^{+}$CD44$^{hi}$CD62L$^{lo}$) were sorted from CD4$^{+}$ cells using a FACS Melody cell sorter (BD Biosciences). Similarly, ILC2s (CD4$^{-}$Lin$^{-}$IL-7Ra$^{+}$Thy1.2$^{+}$) were sorted from Lineage$^{-}$ cells. CD44$^{hi}$CD62L$^{lo}$ T cells were plated onto 48-well tissue culture plates (Costar) that contained IL-2 (15 ng ml$^{-1}$) and recombinant mouse IL-33 (10 ng ml$^{-1}$) and then used as polyclonal Tpath2 cells after 5 d of culture. ILC2s were cultured with recombinant mouse IL-7 (10 U ml$^{-1}$), recombinant mouse IL-25 (10 ng ml$^{-1}$), and recombinant mouse IL-33 (10 ng ml$^{-1}$) for 5 d.

The cell preparation protocol for antigen-specific Tpath2 cells was as follows. Splenic CD62L$^{+}$KJ1$^{+}$CD4$^{+}$ T cells from DO11.10 OVA-specific TCR transgenic mice were stimulated with OVA peptides (Loh15, 0.3 µM) plus antigen-presenting cells (irradiated splenocytes from BALB/c mice) in the presence of IL-2 (25 U ml$^{-1}$), IL-4 (5 ng ml$^{-1}$), and anti-IFNγ monoclonal antibody for 6 d in vitro. The effector Th2 cells ($3 \times 10^{7}$) were transferred intravenously into BALB/c *nu/nu* recipient mice (Fig. S1 A). More than 5 wk after the cell transfer, KJ1$^{+}$CD4$^{+}$ T cells in the spleen were purified by autoMACS (Miltenyi Biotec) and cell sorting (KJ1$^{+}$CD4$^{+}$CXCR3$^{lo}$CD62L$^{lo}$ population; BD FACS Melody or Aria III) and then used as antigen-specific memory Th2 cells. Antigen-specific memory Th2 cells were plated onto 48-well tissue culture plates (Costar) that contained IL-2 (15 ng ml$^{-1}$) and recombinant mouse IL-33 (10 ng ml$^{-1}$) and used as antigen-specific Tpath2 cells after 5 d of culture. For pharmacologic

inhibition of ACC1, TOFA was dissolved in DMSO (10 mM) and administered at a final concentration of 10 µM. For gene deletion of *Acaca*, 4-OHT was added to ERT2-Cre$^{-}$*Acaca*$^{fl/fl}$ or ERT2-Cre$^{+}$*Acaca*$^{fl/fl}$ mouse–derived cells. 4-OHT was dissolved in EtOH (100 µM) and administered at a final concentration of 100 nM.

### Mouse T cell cultures

For the preparation of effector Th2 cells, CD62L$^{+}$CD4$^{+}$ T cells isolated from spleens of C57BL/6J mice were stimulated with plate-coated anti-TCRβ (5 µg ml$^{-1}$) plus anti-CD28 (1 µg ml$^{-1}$) antibodies in complete medium with IL-2 (25 U ml$^{-1}$), IL-4 (5 ng ml$^{-1}$), and anti-IFNγ (1 µg ml$^{-1}$) for 5 d in vitro. To assess IL-3 and GM-CSF production, CD62L$^{+}$CD4$^{+}$ T cells isolated from C57BL/6J mice were cultured for 3 d under the Th2 skewing condition as shown above. For the OA supplementation assay, OA was dissolved in ethanol, with a concentration of 100 mM complexed with 5% BSA before use, and administered to cultured cells at a final concentration 50 µM. Acetate was prepared to 3 M and administered at a final concentration of 5 mM. Glucose was prepared to 0.28 M in complete medium and administered at a final concentration of 50 mM. Curcumin was dissolved in ethanol (10 mM) and administered at a final concentration of 2.5 µM. TSA was dissolved in DMSO (1 mM) and administered at a final concentration of 3 nM.

### Flow cytometry analysis

Cells were analyzed using flow cytometry (FACS Celesta; BD Biosciences). For intracellular cytokine staining, cells were restimulated with PMA (0.1 µg ml$^{-1}$; Sigma-Aldrich) and ionomycin (0.5 µM; Merck) plus monensin (Sigma-Aldrich) for 6 h, followed by fixation and permeabilization. ILC2s were stimulated with IL-7 (10 U ml$^{-1}$)/IL-33 (10 ng ml$^{-1}$) plus monensin (Sigma-Aldrich) for 6 h, followed by fixation and permeabilization. Data were analyzed with FlowJo software (v10.8.0).

### Lung inflammation model

Mice were injected intranasally recombinant mouse IL-33 (100 ng in 20 µl sterile PBS) or papain (50 µg in 20 µl sterile PBS; Nacalai) for three consecutive days. BAL fluid was collected 24 h (papain) or 72 h (IL-33) after last administration. Lung histology and cells were assessed similarly. Mice were immunized with two intraperitoneal injections (days 1 and 8) of 100 µg OVA (dissolved in 100 µl sterile PBS; Sigma-Aldrich) emulsified in alum (100 µl; Thermo Fisher Scientific) and then challenged by intranasal administration of 10 µg OVA dissolved in 20 µl PBS on days 18–22. On day 23 (24 h after final challenge), BAL fluid, lung histology, and cells were analyzed.

### Histopathology

Lung and skin tissues from euthanized mice were fixed in 10% formalin neutral buffer solution (Wako) and embedded in paraffin. H&E- or PAS-stained 5-µm sections were examined with a BZ-X800/X810 fluorescence microscope (Keyence; 20× or 40× objective and zoom of 1.0). Histological analysis was performed with ImageJ (ve1.52n).

### ELISA

Total IgE- and OVA-specific IgE ELISA kits were purchased from BioLegend (432401 and 439807) and used according to the manufacturer's protocol.

### Metabolism analysis

OCR and ECAR were measured with an XF96 analyzer (Agilent Technologies). Memory Th2 cells cultured with IL-33 were seeded at a density of 200,000 cells per well on a microplate. The cells were equilibrated for 1 h in unbuffered XF assay medium supplemented with 25 mM glucose and 1 mM sodium pyruvate before assay. Mixing, waiting, and measure times were 2, 2, and 4 min, respectively. The final concentrations of compounds were 0.2 µM oligomycin, 0.5 µM carbonyl cyanide 4-(trifluoromethoxy) phenylhydrazone, and 0.75 µM rotenone-antimycin-A. The details of cell preparation were previously described (Endo et al., 2019)

### Immunoblotting assay

Th2 cells were washed with PBS and lysed with NE-PER Nuclear and Cytoplasmic Extraction Reagents (Thermo Fisher Scientific) according to the manufacturer's protocol. After debris were centrifugated for 10 min at 20,000 *g* and 4°C, the protein concentration in the lysates of the nuclear fraction was measured with protein assay dye reagent concentrate (Bio-Rad). The antibodies used for the immunoblot analysis were anti-Ac H3K9 (CST) and anti-total H3 (BioLegend). Immunoblotting was performed essentially as previously described (Yamamoto et al., 2018).

### RNA-seq and bioinformatic analysis

Total cellular RNA was extracted with TRIzol reagent (Invitrogen). For cDNA library construction, we used TruSeq RNA Sample Prep Kit v2 (Illumina) according to the manufacturer's protocol. Sequencing the library fragments was performed on the HiSeq 2500 system. For data analysis, read sequences (50 bp) were aligned to the mm10 mouse reference genome (University of California Santa Cruz, December 2011) using Bowtie (v0.12.8) and TopHat (v1.3.2). Fragments per kilobase of exon per million mapped reads (FPKM) for each gene were calculated using Cufflinks (v2.0.2). Genes with an absolute FPKM >1 (mean from duplicate samples) were defined as expressed genes. Gene set enrichment analysis was performed to determine the statistical significance of the enrichment of known transcriptional signatures in a ranked list of genes. We used 2,178 gene sets from the Molecular Signature Database C5 v3.0. Raw and processed sequencing data are available under GEO accession no. GSE185743.

### PCR genotyping for detection of ACC1 deletion

PCR genotyping was performed by using the following primers: forward, 5′-AAGTCCTCAAGGAGCTGGACA-3′, and reverse, 5′-CCACTGCAATTCAGTCACCATC-3′. These primers were designed to sandwich loxp sites, as in a previous study (Mao et al., 2006).

### MC903-induced skin inflammation model

MC903 (calcipotriol; MCE) was dissolved in ethanol (EtOH) and topically applied on mouse ears (2 nmol in 20 µl per ear). CP-640186 was dissolved in EtOH and topically applied on mouse ears (200 nmol in 20 µl per ear). Rapamycin was dissolved in EtOH and topically applied on mouse ears (1 nmol in 20 µl per ear). The same volume of EtOH was used as vehicle control. 4-OHT (Sigma-Aldrich) was dissolved in EtOH (50 µg in 20 µl). MC903, CP-640186, and rapamycin were administered daily, and 4-OHT was administered on days 1, 3, 6, and 8. 6 h after MC903 treatment, 4-OHT, CP-640186, or rapamycin was applied in the same volume as MC903 on ears. Ear thickness was measured daily with a caliper-type digital micrometer (Mitutoyo Corp.). A quarter of the ear was snap-frozen into liquid nitrogen for RNA isolation and extracted with TRIZOL reagent. Mouse recombinant IL-3 (Peprotech) was mixed with anti-IL-3 antibody (BioLegend) to prolong the biological half-life. To prepare IL-3 mixture for injection, IL-3 was mixed with anti-IL-3 antibody for 1 min at room temperature and adjusted to 20 µl with PBS (1 µg IL-3 and 5 µg anti-IL-3 per 20 µl), based on published methods (Ohmori et al., 2009).

### Quantitative real-time PCR

Total RNA was isolated with the TRIzol reagent (Invitrogen). cDNA was synthesized using oligo(dT) primers and Superscript II RT (Invitrogen). Quantitative real-time PCR was performed as described previously using a StepOnePlus real-time PCR system. The primers and Roche universal probes used were purchased from Thermo Fisher Scientific and Roche (Table S1). Gene expression was normalized using the *Hprt* mRNA signal or the *18S* ribosomal RNA signal.

### ChIP assay

ChIP assay was performed as described previously (Angela et al., 2016). In brief, 5 × $10^6$ Th2 cells (cultured for 3 d under Th2 skewing conditions) were fixed with 1% paraformaldehyde at 25°C for 10 min. The lysates were sonicated by a Covaris Focused-Ultrasonicator M220. Quantitative real-time PCR was performed on a StepOnePlus real-time PCR system with TB Green Premix Taq II (Takara). The data of H3-K9 acetylation in Th2 cells were obtained from DBTSS (https://dbtss.hgc.jp/). The antibody for the ChIP assay was anti-acetyl histone H3-K9 (CST). The specific primers used in the ChIP assay were *Il3* promotor (*Il3*p): forward, 5′-TCACATTCATGCTCCAGGGC-3′, and reverse, 5′-CTGGAAGCTGTGGGATGGTT-3′; *Il3*-1: forward, 5′-CAGCAG GCAGGGTTCACC-3′, and reverse, 5′-CAGATGACTCTCAAGCCT CAGT-3′; *Il3*-2: forward, 5′-TGAACATGGCCCCAGTCTTC-3′, and reverse, 5′-TGTTTTAGCTGAGGAGGAGTTTCT-3′; and *Hprt* promotor (*Hprt*p): forward, 5′-TCCTCCTCAGACCGCTTTT-3′, and reverse, 5′-TCTGCTGGAGTCCCCTTG-3′.

### Statistical analysis

Data are expressed as mean ± SD. The data were analyzed with Prism (v7.0e; GraphPad). Differences were assessed using two-tailed Student's *t* tests or two-way ANOVA with Sidak's multiple comparisons test. Differences with values of $P < 0.05$ were considered to be significant. Statistical details of experiments are indicated in the figure legends.

### Online supplemental material

Fig. S1 shows the experimental protocol of memory Th2 cells and gating strategy of $ST2^{hi}$ IL-5–producing cells in vivo. Fig. S2 shows that ACC1 controls the development of $ST2^{hi}$ IL-5–producing pathogenic lymphocytes. Fig. S3 shows that ACC1 controls the production of common β cytokines including IL-3 and GM-CSF in memory Th2 cells. Fig. S4 shows that ACC1 controls MC903-induced skin inflammation via IL-3–mediated basophil activation. Fig. S5 shows that acetate promotes chromatin accessibility at the *Il3* locus in *Acaca*$^{-/-}$ Th2 cells. Table S1 shows specific primers and Roche Universal Probes used for quantitative RT-PCR for mouse genes in this study.

## Acknowledgments

This work was supported by grants from the Ministry of Education, Culture, Sports, Science and Technology (MEXT Japan; Grant-in-Aid for Scientific Research on Innovative Areas 18H04665, Scientific Research [B] 20H03455, Scientific Research [S] 26221305 and JP19H05650, and Challenging Research [Exploratory] 20K21618), Japan Agency for Medical Research and Development (AMED; JP21ek0410060), AMED-CREST (JP21gm1210003), the Nakajima Foundation, Terumo Foundation for Life Sciences and Arts, the Tokyo Biochemical Research Foundation, Kato Memorial Bioscience Foundation, the Hamaguchi Foundation for the Advancement of Biochemistry, Suzuken Memorial Foundation, Kanae Foundation for the Promotion of Medical Science, Takeda Science Foundation, Mochida Memorial Foundation for Medical and Pharmaceutical Research, GlaxoSmithKline Japan Research Grant 2019, SENSHIN Medical Research Foundation, Sumitomo Foundation, Koyanagi Foundation, Kishimoto Foundation 2019, Uehara Memorial Foundation, Nakatomi Foundation, Research Foundation for Pharmaceutical Sciences Group A, Cell Science Research Foundation, the Astellas Foundation for Research on Metabolic Disorders, MSD Life Science Foundation, Public Interest Incorporated Foundation, and Nagase Science Technology Foundation.

Author contributions: T. Nakajima, Y. Endo, T. Kanno, D.J. Tumes, and T. Nakayama conceived and directed the project, designed experiments, interpreted the results, and wrote the manuscript. T. Nakajima and Y. Endo designed the project and analyzed main experiments. T. Nakajima, Y. Endo, T. Kanno, S. Yokoyama, S. Sasamoto, H.K. Asou, and O. Ohara developed experimental protocols and performed experiments.

Disclosures: The authors declare no competing interests exist.

Submitted: 22 March 2021
Revised: 12 September 2021
Accepted: 22 October 2021

## References

Aleman, F., H.F. Lim, and P. Nair. 2016. Eosinophilic Endotype of Asthma. *Immunol. Allergy Clin. North Am.* 36:559–568. https://doi.org/10.1016/j.iac.2016.03.006

Angela, M., Y. Endo, H.K. Asou, T. Yamamoto, D.J. Tumes, H. Tokuyama, K. Yokote, and T. Nakayama. 2016. Fatty acid metabolic reprogramming via mTOR-mediated inductions of PPARγ directs early activation of T cells. *Nat. Commun.* 7:13683. https://doi.org/10.1038/ncomms13683

Berod, L., C. Friedrich, A. Nandan, J. Freitag, S. Hagemann, K. Harmrolfs, A. Sandouk, C. Hesse, C.N. Castro, H. Bähre, et al. 2014. De novo fatty acid synthesis controls the fate between regulatory T and T helper 17 cells. *Nat. Med.* 20:1327–1333. https://doi.org/10.1038/nm.3704

Brandt, E.B., and U. Sivaprasad. 2011. Th2 Cytokines and Atopic Dermatitis. *J. Clin. Cell. Immunol.* 2:110. https://doi.org/10.4172/2155-9899.1000110

Broughton, S.E., U. Dhagat, T.R. Hercus, T.L. Nero, M.A. Grimbaldeston, C.S. Bonder, A.F. Lopez, and M.W. Parker. 2012. The GM-CSF/IL-3/IL-5 cytokine receptor family: from ligand recognition to initiation of signaling. *Immunol. Rev.* 250:277–302. https://doi.org/10.1111/j.1600-065X.2012.01164.x

Chapman, N.M., and H. Chi. 2014. mTOR signaling, Tregs and immune modulation. *Immunotherapy.* 6:1295–1311. https://doi.org/10.2217/imt.14.84

Chi, H. 2012. Regulation and function of mTOR signalling in T cell fate decisions. *Nat. Rev. Immunol.* 12:325–338. https://doi.org/10.1038/nri3198

Comerford, S.A., Z. Huang, X. Du, Y. Wang, L. Cai, A.K. Witkiewicz, H. Walters, M.N. Tantawy, A. Fu, H.C. Manning, et al. 2014. Acetate dependence of tumors. *Cell.* 159:1591–1602. https://doi.org/10.1016/j.cell.2014.11.020

Delgoffe, G.M., T.P. Kole, Y. Zheng, P.E. Zarek, K.L. Matthews, B. Xiao, P.F. Worley, S.C. Kozma, and J.D. Powell. 2009. The mTOR kinase differentially regulates effector and regulatory T cell lineage commitment. *Immunity.* 30:832–844. https://doi.org/10.1016/j.immuni.2009.04.014

Dougan, M., G. Dranoff, and S.K. Dougan. 2019. GM-CSF, IL-3, and IL-5 Family of Cytokines: Regulators of Inflammation. *Immunity.* 50:796–811. https://doi.org/10.1016/j.immuni.2019.03.022

Duncliffe, K.N., A.G. Bert, M.A. Vadas, and P.N. Cockerill. 1997. A T cell-specific enhancer in the interleukin-3 locus is activated cooperatively by Oct and NFAT elements within a DNase I-hypersensitive site. *Immunity.* 6:175–185. https://doi.org/10.1016/S1074-7613(00)80424-0

Endo, Y., C. Iwamura, M. Kuwahara, A. Suzuki, K. Sugaya, D.J. Tumes, K. Tokoyoda, H. Hosokawa, M. Yamashita, and T. Nakayama. 2011. Eomesodermin controls interleukin-5 production in memory T helper 2 cells through inhibition of activity of the transcription factor GATA3. *Immunity.* 35:733–745. https://doi.org/10.1016/j.immuni.2011.08.017

Endo, Y., K. Hirahara, R. Yagi, D.J. Tumes, and T. Nakayama. 2014. Pathogenic memory type Th2 cells in allergic inflammation. *Trends Immunol.* 35:69–78. https://doi.org/10.1016/j.it.2013.11.003

Endo, Y., H.K. Asou, N. Matsugae, K. Hirahara, K. Shinoda, D.J. Tumes, H. Tokuyama, K. Yokote, and T. Nakayama. 2015a. Obesity Drives Th17 Cell Differentiation by Inducing the Lipid Metabolic Kinase, ACC1. *Cell Rep.* 12:1042–1055. https://doi.org/10.1016/j.celrep.2015.07.014

Endo, Y., K. Hirahara, T. Iinuma, K. Shinoda, D.J. Tumes, H.K. Asou, N. Matsugae, K. Obata-Ninomiya, H. Yamamoto, S. Motohashi, et al. 2015b. The interleukin-33-p38 kinase axis confers memory T helper 2 cell pathogenicity in the airway. *Immunity.* 42:294–308. https://doi.org/10.1016/j.immuni.2015.01.016

Endo, Y., A. Onodera, K. Obata-Ninomiya, R. Koyama-Nasu, H.K. Asou, T. Ito, T. Yamamoto, T. Kanno, T. Nakajima, K. Ishiwata, et al. 2019. ACC1 determines memory potential of individual CD4$^+$ T cells by regulating de novo fatty acid biosynthesis. *Nat. Metab.* 1:261–275. https://doi.org/10.1038/s42255-018-0025-4

Fahy, J.V. 2015. Type 2 inflammation in asthma--present in most, absent in many. *Nat. Rev. Immunol.* 15:57–65. https://doi.org/10.1038/nri3786

Finkelman, F.D., K.B. Madden, S.C. Morris, J.M. Holmes, N. Boiani, I.M. Katona, and C.R. Maliszewski. 1993. Anti-cytokine antibodies as carrier proteins. Prolongation of in vivo effects of exogenous cytokines by injection of cytokine-anti-cytokine antibody complexes. *J. Immunol.* 151:1235–1244.

Furusawa, Y., Y. Obata, S. Fukuda, T.A. Endo, G. Nakato, D. Takahashi, Y. Nakanishi, C. Uetake, K. Kato, T. Kato, et al. 2013. Commensal microbe-derived butyrate induces the differentiation of colonic regulatory T cells. *Nature.* 504:446–450. https://doi.org/10.1038/nature12721

Gour, N., and M. Wills-Karp. 2015. IL-4 and IL-13 signaling in allergic airway disease. *Cytokine.* 75:68–78. https://doi.org/10.1016/j.cyto.2015.05.014

Guttman-Yassky, E., K.E. Nograles, and J.G. Krueger. 2011. Contrasting pathogenesis of atopic dermatitis and psoriasis--part II: immune cell subsets and therapeutic concepts. *J. Allergy Clin. Immunol.* 127:1420–1432. https://doi.org/10.1016/j.jaci.2011.01.054

Halim, T.Y., C.A. Steer, L. Mathä, M.J. Gold, I. Martinez-Gonzalez, K.M. McNagny, A.N. McKenzie, and F. Takei. 2014. Group 2 innate lymphoid cells are critical for the initiation of adaptive T helper 2 cell-mediated allergic lung inflammation. *Immunity.* 40:425–435. https://doi.org/10.1016/j.immuni.2014.01.011

Holgate, S.T. 2012. Innate and adaptive immune responses in asthma. *Nat. Med.* 18:673–683. https://doi.org/10.1038/nm.2731

Islam, S.A., D.S. Chang, R.A. Colvin, M.H. Byrne, M.L. McCully, B. Moser, S.A. Lira, I.F. Charo, and A.D. Luster. 2011. Mouse CCL8, a CCR8 agonist, promotes atopic dermatitis by recruiting IL-5+ T(H)2 cells. *Nat. Immunol.* 12:167–177. https://doi.org/10.1038/ni.1984

Ito, Y., T. Satoh, K. Takayama, C. Miyagishi, A.F. Walls, and H. Yokozeki. 2011. Basophil recruitment and activation in inflammatory skin diseases. *Allergy.* 66:1107–1113. https://doi.org/10.1111/j.1398-9995.2011.02570.x

Jewell, J.L., and K.L. Guan. 2013. Nutrient signaling to mTOR and cell growth. *Trends Biochem. Sci.* 38:233–242. https://doi.org/10.1016/j.tibs.2013.01.004

Karagiannis, F., S.K. Masouleh, K. Wunderling, J. Surendar, V. Schmitt, A. Kazakov, M. Michla, M. Hölzel, C. Thiele, and C. Wilhelm. 2020. Lipid-Droplet Formation Drives Pathogenic Group 2 Innate Lymphoid Cells in Airway Inflammation. *Immunity.* 52:620–634.e6. https://doi.org/10.1016/j.immuni.2020.03.003

Kidani, Y., H. Elsaesser, M.B. Hock, L. Vergnes, K.J. Williams, J.P. Argus, B.N. Marbois, E. Komisopoulou, E.B. Wilson, T.F. Osborne, et al. 2013. Sterol regulatory element-binding proteins are essential for the metabolic programming of effector T cells and adaptive immunity. *Nat. Immunol.* 14:489–499. https://doi.org/10.1038/ni.2570

Lee, J., M.C. Walsh, K.L. Hoehn, D.E. James, E.J. Wherry, and Y. Choi. 2014. Regulator of fatty acid metabolism, acetyl coenzyme a carboxylase 1, controls T cell immunity. *J. Immunol.* 192:3190–3199. https://doi.org/10.4049/jimmunol.1302985

Leyva-Castillo, J.M., P. Hener, P. Michea, H. Karasuyama, S. Chan, V. Soumelis, and M. Li. 2013. Skin thymic stromal lymphopoietin initiates Th2 responses through an orchestrated immune cascade. *Nat. Commun.* 4:2847. https://doi.org/10.1038/ncomms3847

Lotfi, N., R. Thome, N. Rezaei, G.X. Zhang, A. Rezaei, A. Rostami, and N. Esmaeil. 2019. Roles of GM-CSF in the Pathogenesis of Autoimmune Diseases: An Update. *Front. Immunol.* 10:1265. https://doi.org/10.3389/fimmu.2019.01265

Maddur, M.S., P. Miossec, S.V. Kaveri, and J. Bayry. 2012. Th17 cells: biology, pathogenesis of autoimmune and inflammatory diseases, and therapeutic strategies. *Am. J. Pathol.* 181:8–18. https://doi.org/10.1016/j.ajpath.2012.03.044

Mao, J., F.J. DeMayo, H. Li, L. Abu-Elheiga, Z. Gu, T.E. Shaikenov, P. Kordari, S.S. Chirala, W.C. Heird, and S.J. Wakil. 2006. Liver-specific deletion of acetyl-CoA carboxylase 1 reduces hepatic triglyceride accumulation without affecting glucose homeostasis. *Proc. Natl. Acad. Sci. USA.* 103:8552–8557. https://doi.org/10.1073/pnas.0603115103

Monticelli, L.A., M.D. Buck, A.L. Flamar, S.A. Saenz, E.D. Tait Wojno, N.A. Yudanin, L.C. Osborne, M.R. Hepworth, S.V. Tran, H.R. Rodewald, et al. 2016. Arginase 1 is an innate lymphoid-cell-intrinsic metabolic checkpoint controlling type 2 inflammation. *Nat. Immunol.* 17:656–665. https://doi.org/10.1038/ni.3421

Murphy, K.M., A.B. Heimberger, and D.Y. Loh. 1990. Induction by antigen of intrathymic apoptosis of CD4+CD8+TCRlo thymocytes in vivo. *Science.* 250:1720–1723. https://doi.org/10.1126/science.2125367

Nakayama, T., K. Hirahara, A. Onodera, Y. Endo, H. Hosokawa, K. Shinoda, D.J. Tumes, and Y. Okamoto. 2017. Th2 Cells in Health and Disease. *Annu. Rev. Immunol.* 35:53–84. https://doi.org/10.1146/annurev-immunol-051116-052350

Ohmori, K., Y. Luo, Y. Jia, J. Nishida, Z. Wang, K.D. Bunting, D. Wang, and H. Huang. 2009. IL-3 induces basophil expansion in vivo by directing granulocyte-monocyte progenitors to differentiate into basophil lineage-restricted progenitors in the bone marrow and by increasing the number of basophil/mast cell progenitors in the spleen. *J. Immunol.* 182:2835–2841. https://doi.org/10.4049/jimmunol.0802870

Pan, Y., T. Tian, C.O. Park, S.Y. Lofftus, S. Mei, X. Liu, C. Luo, J.T. O'Malley, A. Gehad, J.E. Teague, et al. 2017. Survival of tissue-resident memory T cells requires exogenous lipid uptake and metabolism. *Nature.* 543:252–256. https://doi.org/10.1038/nature21379

Pollizzi, K.N., and J.D. Powell. 2014. Integrating canonical and metabolic signalling programmes in the regulation of T cell responses. *Nat. Rev. Immunol.* 14:435–446. https://doi.org/10.1038/nri3701

Qiu, J., M. Villa, D.E. Sanin, M.D. Buck, D. O'Sullivan, R. Ching, M. Matsushita, K.M. Grzes, F. Winkler, C.H. Chang, et al. 2019. Acetate Promotes T Cell Effector Function during Glucose Restriction. *Cell Rep.* 27:2063–2074.e5. https://doi.org/10.1016/j.celrep.2019.04.022

Salmond, R.J., A.S. Mirchandani, A.G. Besnard, C.C. Bain, N.C. Thomson, and F.Y. Liew. 2012. IL-33 induces innate lymphoid cell-mediated airway inflammation by activating mammalian target of rapamycin. *J. Allergy*

*Clin. Immunol.* 130:1159–1166.e6. https://doi.org/10.1016/j.jaci.2012.05.018

Saravia, J., N.M. Chapman, and H. Chi. 2019. Helper T cell differentiation. *Cell. Mol. Immunol.* 16:634–643. https://doi.org/10.1038/s41423-019-0220-6

Saxton, R.A., and D.M. Sabatini. 2017. mTOR Signaling in Growth, Metabolism, and Disease. *Cell.* 168:960–976. https://doi.org/10.1016/j.cell.2017.02.004

Siracusa, M.C., B.S. Kim, J.M. Spergel, and D. Artis. 2013. Basophils and allergic inflammation. *J. Allergy Clin. Immunol.* 132:789–801, quiz :788. https://doi.org/10.1016/j.jaci.2013.07.046

Slack, M., T. Wang, and R. Wang. 2015. T cell metabolic reprogramming and plasticity. *Mol. Immunol.* 68(2, 2 Pt C):507–512. https://doi.org/10.1016/j.molimm.2015.07.036

Stark, J.M., C.A. Tibbitt, and J.M. Coquet. 2019. The Metabolic Requirements of Th2 Cell Differentiation. *Front. Immunol.* 10:2318. https://doi.org/10.3389/fimmu.2019.02318

van der Windt, G.J.W., C.H. Chang, and E.L. Pearce. 2016. Measuring Bioenergetics in T Cells Using a Seahorse Extracellular Flux Analyzer. *Curr. Protoc. Immunol.* 113:1: 14. https://doi.org/10.1002/0471142735.im0316bs113

Vodnala, S.K., R. Eil, R.J. Kishton, M. Sukumar, T.N. Yamamoto, N.H. Ha, P.H. Lee, M. Shin, S.J. Patel, Z. Yu, et al. 2019. T cell stemness and dysfunction in tumors are triggered by a common mechanism. *Science.* 363:eaau0135. https://doi.org/10.1126/science.aau0135

Walker, J.A., and A.N.J. McKenzie. 2018. $T_H2$ cell development and function. *Nat. Rev. Immunol.* 18:121–133. https://doi.org/10.1038/nri.2017.118

Weichhart, T., M. Hengstschläger, and M. Linke. 2015. Regulation of innate immune cell function by mTOR. *Nat. Rev. Immunol.* 15:599–614. https://doi.org/10.1038/nri3901

Yamamoto, T., Y. Endo, A. Onodera, K. Hirahara, H.K. Asou, T. Nakajima, T. Kanno, Y. Ouchi, S. Uematsu, H. Nishimasu, et al. 2018. DUSP10 constrains innate IL-33-mediated cytokine production in $ST2^{hi}$ memory-type pathogenic Th2 cells. *Nat. Commun.* 9:4231. https://doi.org/10.1038/s41467-018-06468-8

Yang, K., S. Shrestha, H. Zeng, P.W. Karmaus, G. Neale, P. Vogel, D.A. Guertin, R.F. Lamb, and H. Chi. 2013. T cell exit from quiescence and differentiation into Th2 cells depend on Raptor-mTORC1-mediated metabolic reprogramming. *Immunity.* 39:1043–1056. https://doi.org/10.1016/j.immuni.2013.09.015

Yao, C.H., R. Fowle-Grider, N.G. Mahieu, G.Y. Liu, Y.J. Chen, R. Wang, M. Singh, G.S. Potter, R.W. Gross, J. Schaefer, et al. 2016. Exogenous Fatty Acids Are the Preferred Source of Membrane Lipids in Proliferating Fibroblasts. *Cell Chem. Biol.* 23:483–493. https://doi.org/10.1016/j.chembiol.2016.03.007

## Supplemental material

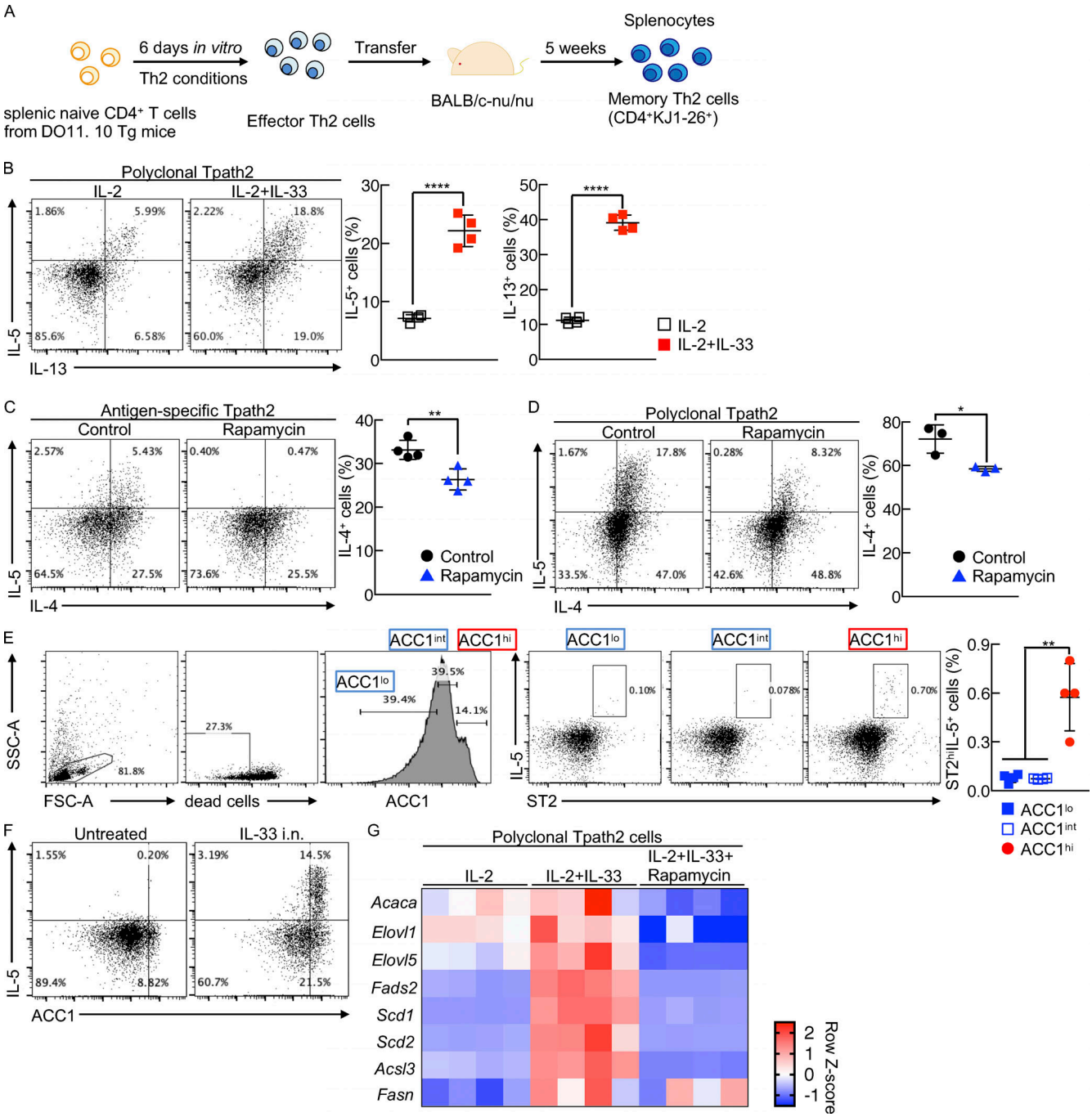


Figure S1. **Experimental protocol of memory Th2 cells and gating strategy of ST2$^{hi}$ IL-5–producing cells in vivo. (A)** Experimental protocol for the generation of memory Th2 cell. **(B)** Intracellular staining profiles of IL-5 and IL-13 in restimulated polyclonal Tpath2 cells. The percentages of IL-5$^+$ and IL-13$^+$ cells are shown with SD. Cells were cultured with IL-2 or IL-2 plus IL-33 in complete medium for 5 d. **(C and D)** Intracellular staining profiles of IL-5 and IL-4 in restimulated antigen-specific Tpath2 cells (C) or polyclonal Tpath2 cells (D) treated with or without rapamycin (100 nM). The percentages of IL-4$^+$ cells are shown with SD. Cells were cultured with IL-33 (B) or IL-2 and IL-33 (C) in complete medium for 5 d. **(E)** Intracellular staining profiles and gating strategy for flow cytometric analysis of lung cells that express ACC1 low, intermediate, and high cells. Intracellular staining profiles of IL-5 and ST2 in each population. The percentages of ST2$^{hi}$IL-5$^+$ cells are shown with SD. FSC, forward scatter; SSC, side scatter. **(F)** Representative intracellular staining profiles of ACC1 and IL-5 in restimulated lung lymphocytes isolated from untreated C57BL/6 mice or C57BL/6 mice administered IL-33 intranasally. **(G)** Heatmap visualization of expression profiles of genes involved in fatty acid biosynthesis in IL-2–cultured and IL-2 plus IL-33–cultured polyclonal Tpath2 cells treated with or without rapamycin. The Z-score scales ranging from blue to red are shown in the bottom right corner. For each group, $n = 3$ (D) or 4 (B, C, and E–G) biologically independent samples are shown. More than three independent experiments were performed with similar results for B–G. Mean values with SD are shown for B–E. An unpaired two-tailed Student's $t$ test was applied for B–E. Statistical significance (P values) is indicated as *, P < 0.05; **, P < 0.01; ****, P < 0.0001.

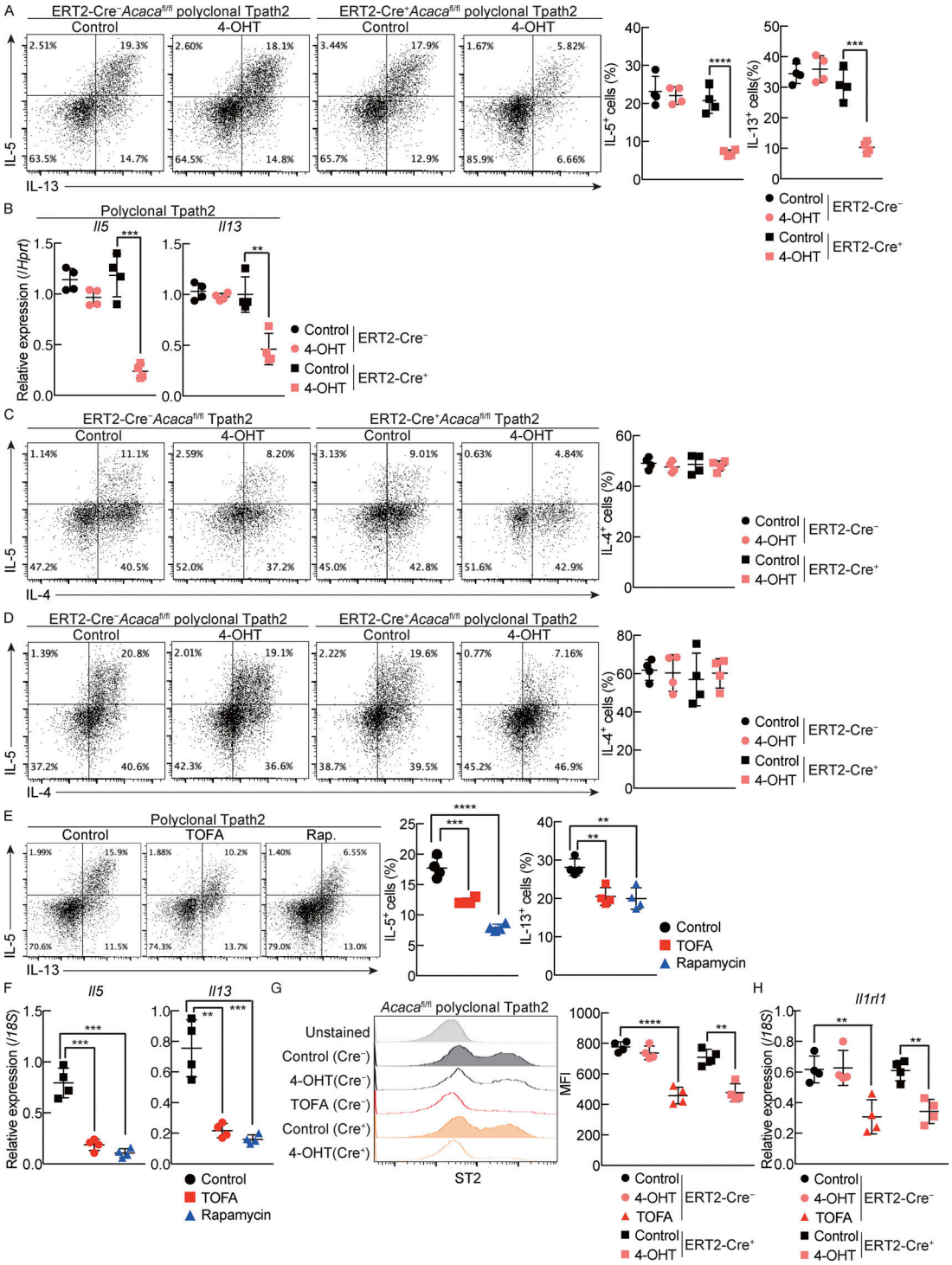


Figure S2. **ACC1 controls the development of ST2$^{hi}$ IL-5–producing pathogenic lymphocytes. (A and D)** Intracellular staining profiles of IL-5 and IL-13 (A) or IL-5 and IL-4 (D) in restimulated ERT2-Cre$^{-}$*Acaca*$^{fl/fl}$ or ERT2-Cre$^{+}$*Acaca*$^{fl/fl}$ polyclonal Tpath2 cells treated with or without 4-OHT. The percentages of IL-5$^{+}$ and IL-13$^{+}$ cells (A) or IL-4$^{+}$ cells (D) are shown. **(B)** Quantitative RT-PCR analysis of *Il5* and *Il13* in ERT2-Cre$^{-}$*Acaca*$^{fl/fl}$ or ERT2-Cre$^{+}$*Acaca*$^{fl/fl}$ polyclonal Tpath2 cells treated with or without 4-OHT. **(C)** Intracellular staining profiles of IL-5 and IL-4 in restimulated ERT2-Cre$^{-}$*Acaca*$^{fl/fl}$ or ERT2-Cre$^{+}$*Acaca*$^{fl/fl}$ Tpath2 cells treated with or without 4-OHT. The percentages of IL-4$^{+}$ cells are shown. **(E)** Intracellular staining profiles of IL-5 and IL-13 in restimulated polyclonal Tpath2 cells treated with TOFA or rapamycin. The percentages of IL-5$^{+}$ and IL-13$^{+}$ cells are shown. **(F)** Quantitative RT-PCR analysis of *Il5* and *Il13* in polyclonal Tpath2 cells treated with TOFA or rapamycin. **(G)** Expression profiles of ST2 on ERT2-Cre$^{-}$*Acaca*$^{fl/fl}$ or ERT2-Cre$^{+}$*Acaca*$^{fl/fl}$ polyclonal Tpath2 cells treated with 4-OHT or TOFA on day 5. The graph shows mean fluorescence intensity (MFI) ± SD values of ST2 in each group. **(H)** Quantitative RT-PCR analysis of *Il1rl1* in ERT2-Cre$^{-}$*Acaca*$^{fl/fl}$ or ERT2-Cre$^{+}$*Acaca*$^{fl/fl}$ polyclonal Tpath2 cells treated with 4-OHT or TOFA. For each group, $n$ = 4 biologically independent samples are shown (A–H). The cells isolated from ERT2-Cre$^{-}$*Acaca*$^{fl/fl}$ or ERT2-Cre$^{+}$*Acaca*$^{fl/fl}$ mice were used for A–D, G, and H. More than three independent experiments were performed with similar results for A–H. Mean values with SD are shown for A–H. An unpaired two-tailed Student's $t$ test was applied for A–H. Statistical significance (P values) is indicated as **, P < 0.01; ***, P < 0.001; ****, P < 0.0001.

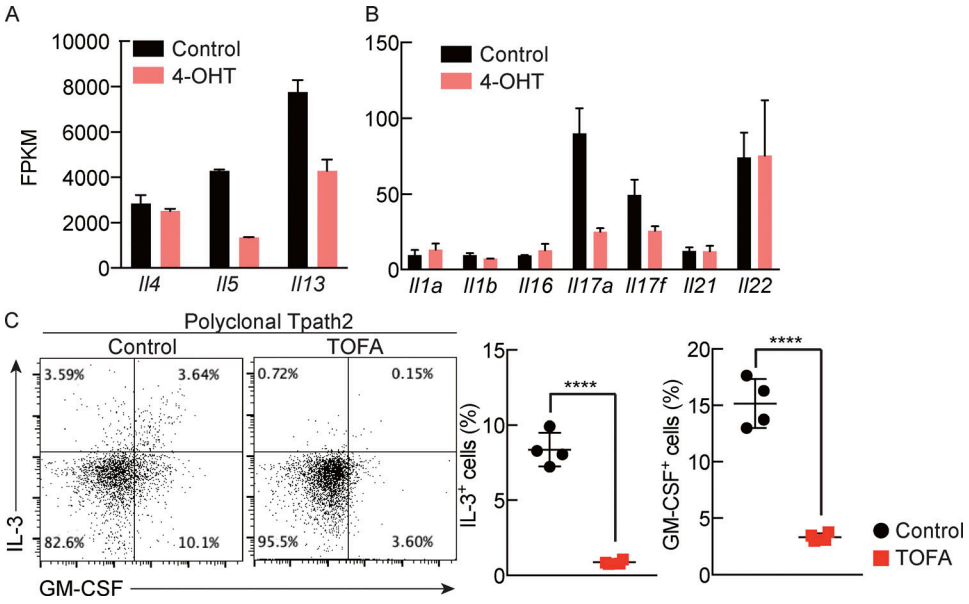


Figure S3. **ACC1 controls the production of common β cytokines, including IL-3 and GM-CSF, in memory Th2 cells. (A and B)** Expression profile by RNA-seq of selected cytokine genes in Tpath2 cells. **(C)** Intracellular staining profiles of IL-3 and GM-CSF in restimulated polyclonal Tpath2 cells treated with or without TOFA. The percentages of IL-3$^+$ cells or GM-CSF$^+$ cells are shown with SD. For each group, $n = 2$ (A and B) or 4 (C) biologically independent samples are shown. More than three independent experiments were performed with similar results for C. Mean values with SD are shown for C. An unpaired two-tailed Student's *t* test was applied for C. Statistical significance (P values) is indicated as ****, P < 0.0001.

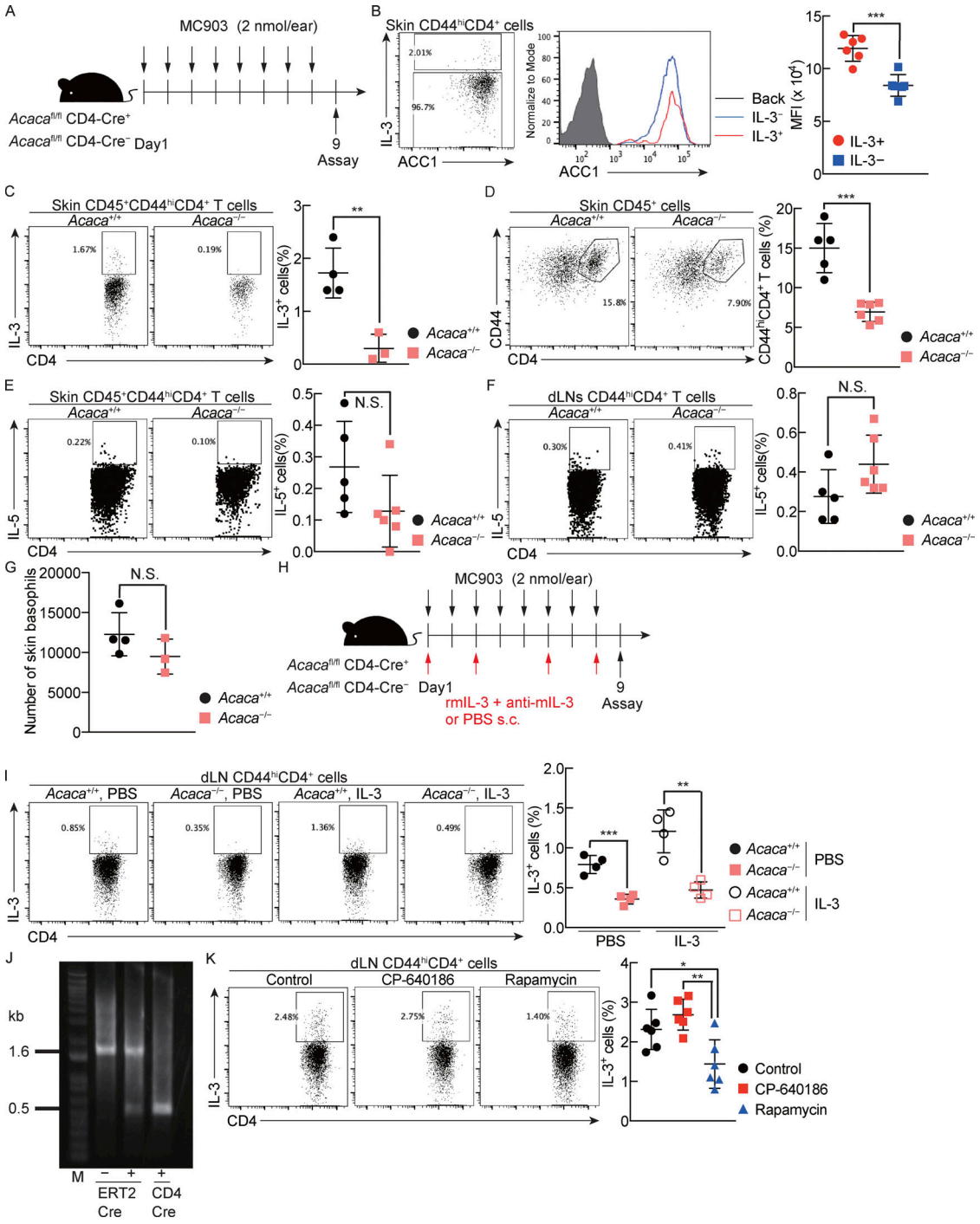


Figure S4. **ACC1 controls MC903-induced skin inflammation via IL-3–mediated basophil activation. (A)** Experimental protocol for MC903-induced skin inflammation model. 1 nmol MC903 in 10 µl EtOH was applied topically on both sides of ear (total 2 nmol/20 µl per ear). **(B)** Intracellular staining profiles of IL-3 and ACC1 in ear CD45$^+$CD44$^{hi}$CD4$^+$ T cells. Histogram shows ACC1 expression of IL-3$^+$ or IL-3$^-$ cells. Gray filled histogram indicates background, stained without primary antibody. **(C)** Intracellular staining profiles of IL-3 in ear CD45$^+$CD44$^{hi}$CD4$^+$ T cells. The percentage of IL-3$^+$ cells is shown. **(D)** Expression profiles of CD4 and CD44 on *Acaca*$^{+/+}$ or *Acaca*$^{-/-}$ skin CD45$^+$ cells. **(E and F)** Intracellular staining profiles of IL-5 in ear (E) or ear-dLN (F) CD45$^+$CD44$^{hi}$CD4$^+$ T cells. The percentage of IL-5$^+$ cells is shown. **(G)** The absolute number of skin basophils in *Acaca*$^{+/+}$ or *Acaca*$^{-/-}$ mice. **(H)** Experimental protocol for MC903-induced skin inflammation model with subcutaneous injection of mIL-3/anti-mIL-3 mixture or PBS. IL-3 mixture or PBS administration was performed on days 1, 3, 6, and 8 (details of reagent in Materials and methods). **(I)** Intracellular staining profiles of IL-3 in ear dLN CD44$^{hi}$CD4$^+$ T cells. The percentage of IL-3$^+$ cells is shown. **(J)** Confirmation of gene depletion in cells by tamoxifen-inducible and CD4-specific deletion of *Acaca*. PCR analysis indicates *Acaca* deletion in genomic DNA of ear CD45$^+$ cells (ERT-Cre$^+$ or ERT-Cre$^-$) and lymph-node CD4$^+$ cells (as positive control). Representative data are shown. **(K)** Intracellular staining profiles of IL-3 in stimulated ear CD45$^+$CD44$^{hi}$CD4$^+$ T cells. The percentage of IL-3$^+$ cells is shown. For each group, $n$ = 3–4 (C and G); 4 (I and J); 5–6 (D–F); or 6 (B and K) biologically independent samples are shown. More than three independent experiments were performed with similar results for B–G and I–K. An unpaired two-tailed Student's $t$ test was applied for B–G, I, and K. Mean values with SD are shown for B–G, I, and K. Statistical significance (P values) is indicated as *, P < 0.05; **, P < 0.01; ***, P < 0.001; N.S., not significant.

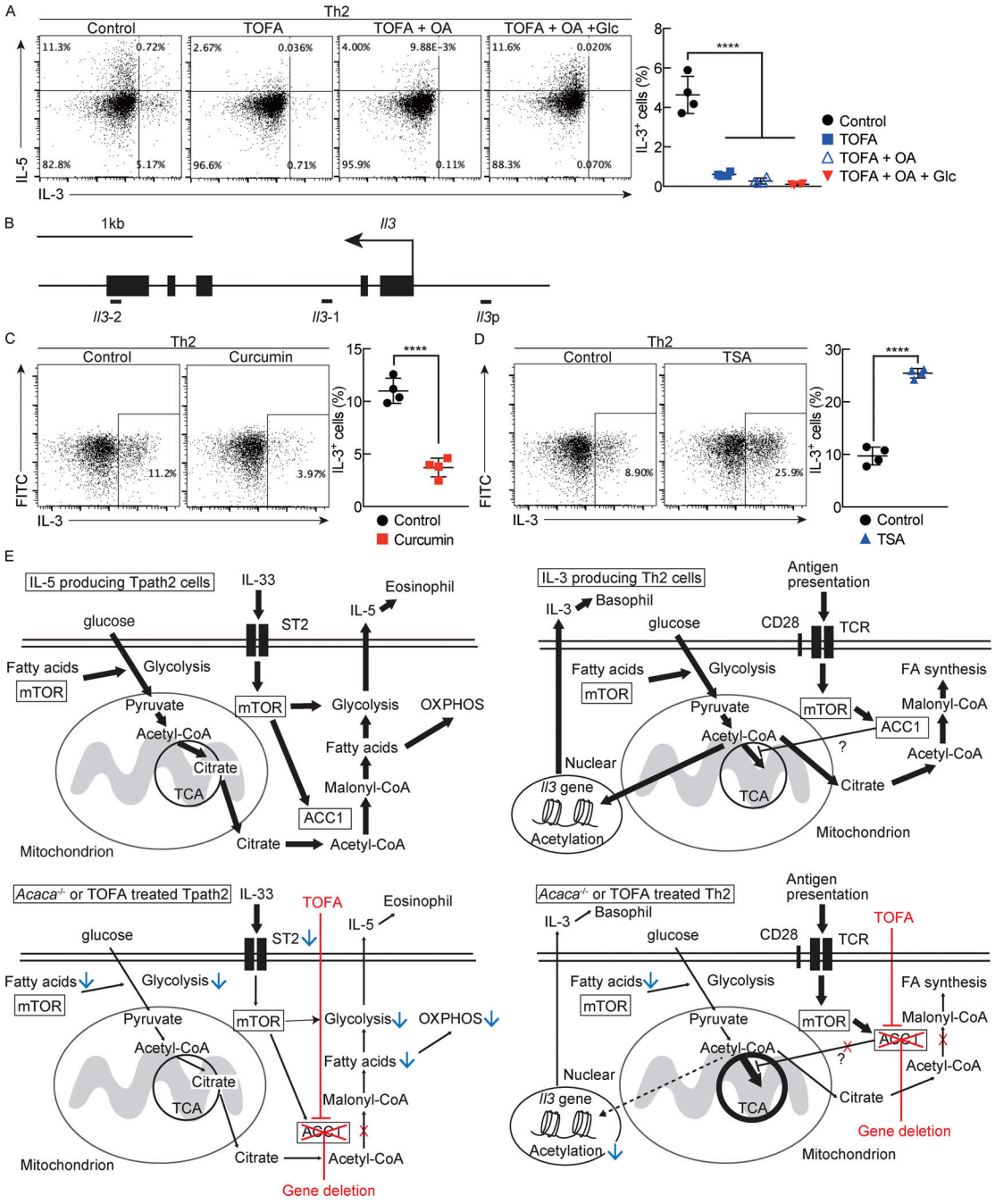


Figure S5. **Acetate promotes chromatin accessibility at the *Il3* locus in *Acaca*$^{-/-}$ Th2 cells. (A)** Intracellular staining profiles of IL-5 and IL-3 in restimulated Th2 cells treated with TOFA in the presence or absence of OA (50 µM) and glucose (50 mM). The percentage of IL-3$^+$ cells is shown with SD. **(B)** Schematic representation of the murine *Il3* locus. The locations of primers and exons are indicated. **(C)** Intracellular staining profiles of IL-3 in restimulated Th2 cells treated with or without Curcumin (2.5 µM). The percentage of IL-3$^+$ cells is shown with SD. **(D)** Intracellular staining profiles of IL-3 in restimulated Th2 cells treated with or without TSA (3 nM). The percentage of IL-3$^+$ cells is shown with SD. **(E)** Upper left: IL-33 stimulation induces fatty acid biosynthesis via the mTORC1-ACC1 axis in IL-5–producing Tpath2 cells. Fatty acid biosynthesis and maximal glycolytic capacity control a large amount of IL-5 production and eosinophilic inflammation in the lung. OXPHOS, oxidative phosphorylation; TCA, tricarboxylic acid. Lower left: Fatty acid biosynthesis in Tpath2 cells is inhibited by genetic deletion or pharmacologic inhibition of ACC1. Blockade of de novo fatty acid biosynthesis reduced glycolysis, which resulted in a dramatic decrease of IL-5 production in Tpath2 cells. Upper right: Antigenic TCR stimulation induces fatty acid (FA) biosynthesis via the mTORC1-ACC1 axis in IL-3–producing Th2 cells. Active fatty acid biosynthesis properly regulates the availability of cellular Ac-CoA into histone acetylation and induces IL-3 production in Th2 cells. Lower right: Fatty acid biosynthesis is suppressed by genetic deletion or pharmacologic inhibition of ACC1 in Th2 cells. As a result, cellular Ac-CoA likely feeds into the cellular pool of metabolites in the tricarboxylic acid cycle, which may decrease the usage of Ac-CoA for chromatin acetylation. The reduction of histone acetylation levels at the *Il3* gene locus in *Acaca*$^{-/-}$ or TOFA-treated Th2 cells strongly decreases transcription and production of IL-3. For each group, $n = 4$ biologically independent samples are shown (A, C, and D). More than three independent experiments were performed with similar results for A, C, and D. Mean values with SD are shown for A, C, and D. An unpaired two-tailed Student's *t* test was applied for A, C, and D. Statistical significance (P values) is indicated as ****, $P < 0.0001$.

**Table S1 is provided online as an Excel file and shows specific primers and Roche Universal Probes used for quantitative RT-PCR of mouse genes.**